

Automating Lung Cancer Identification in PET/CT Imaging

BY

ELEONORA D'ARNESE

B.S, Politecnico di Milano, Milan, Italy, 2016

THESIS

Submitted as partial fulfillment of the requirements
for the degree of Master of Science in BioEngineering
in the Graduate College of the
University of Illinois at Chicago, 2018

Chicago, Illinois

Defense Committee:

Tanya Berger-Wolf, Chair and Advisor

Robert V. Kenyon

Marco D. Santambrogio, Politecnico di Milano

ACKNOWLEDGMENTS

This work has been made possible thanks to several people that thanks to their time, support and patience have helped me throughout this period. Firstly, I want to thank Marco Domenico Santambrogio, who helped and encouraged me in the last years; who with his guidance this thesis has been possible. A thank you also goes to Emanuele Del Sozzo for his time and the help that he gave me in this project. Thank you also to all the people working in the NECSTLab at Politecnico di Milano, that created a friendly, stimulating and challenging environment sharing expertise and suggestions. Thanks to Tanya Berger-Wolf and to all the members of the CompPopBio Lab for the time spent together and the knowledge that they have shared. A great thank you to the PoliMi-UIC students of Fall 2017 who shared with me this magnificent experience during all these months. Last but not least, I want to express my appreciation and affection to my parents for the support, encouragement and the chance they gave me to live this experience.

ED

TABLE OF CONTENTS

<u>CHAPTER</u>	<u>PAGE</u>
1 INTRODUCTION AND MOTIVATION	1
1.1 Thesis goal	4
1.2 Outline	4
2 BACKGROUND	6
2.1 Respiratory apparatus anatomy	6
2.2 Investigated pathology	8
2.3 Imaging techniques	11
2.3.1 Computed Tomography	11
2.3.2 Positron Emission Tomography	13
3 RELATED WORK	17
3.1 Invasive vs non-invasive assessment techniques	17
3.2 Segmentation methods	20
3.2.1 Neural Networks	20
3.2.2 Watershed algorithm	22
3.2.3 Graph-based approach	22
3.2.4 Morphologic and filtering approach	23
3.3 Data availability and evaluation challenges	23
3.4 Summary	24
4 PROBLEM STATEMENT AND GOALS	26
4.1 Problem definition	26
4.2 Thesis objective	27
5 METHODOLOGY	30
5.1 Proposed pipeline overview	30
5.2 Dataset description	32
5.3 CT preprocessing	34
5.4 Lungs segmentation	38
5.5 PET processing	41
5.6 CT and PET fusion	43
6 IMPLEMENTATION	47
6.1 Technical details	47
6.2 Dataset structure	49
6.3 CT preprocessing	51

TABLE OF CONTENTS (continued)

<u>CHAPTER</u>		<u>PAGE</u>
	6.4 CT analysis	52
	6.5 PET analysis	56
	6.6 Cancer lesion identification	58
7	EXPERIMENTAL EVALUATION	64
	7.1 Experimental setup	64
	7.2 Execution time	65
	7.3 Accuracy	66
8	CONCLUSIONS AND FUTURE WORKS	70
	APPENDICES	73
	Appendix A	74
	Appendix B	75
	CITED LITERATURE	76
	VITA	83

LIST OF TABLES

<u>TABLE</u>		<u>PAGE</u>
I	RELEVANT DETAILS ABOUT THE DATASET ANALYZED .	48

LIST OF FIGURES

<u>FIGURE</u>		<u>PAGE</u>
1	Diagram of lobes of the human lungs	7
2	Representation of cancer cells spreading through healthy tissue . . .	8
3	Basic scheme of Computed Tomography	13
4	Basic scheme of Positron Emission Tomography	15
5	Scheme of the implemented pipeline	31
6	8-connectivity representation	39
7	4-connectivity representation	45
8	Dataset composition divided by acquisition method and cancer type, where STD= <i>standard acquisition</i> , HEL= <i>helical acquisition</i> , SQC= <i>squamous lung cancer</i> and ADK= <i>adenocarcinoma lung cancer</i> . . .	49
9	Contrast adjustment with linear gamma correction	50
10	Sobel vs Canny edge detection approaches	51
11	Creation of the mask that will be employed for the removal of the gantry artifact	53
12	Identification of the largest connected component based on the 8- connectivity filter	54
13	From the input to the background and thorax removal within the lungs identification process	55
14	Morphological closure with different constructing element radius; the green one is the selected one	56
15	Identification of the Region of Interest within the CT processing pipeline	57
16	Removal of PET centroid based on the CT corresponding values . .	59
17	Identification of the valid centroid inside the Region of Interest . . .	61
18	Final identification of the contour of the lungs cancer lesion	62
19	Execution time on different dataset dimensions	65
20	Accuracy obtained for each patient considering the number of ana- lyzed images (the number of images is reported above each bar) . .	67
21	Number of correctly classified vs misclassified patients	68

List of Algorithms

1	Pseudocode of the CT acquisition method	35
2	Pseudocode for the Otsu's method	37
3	Pseudocode for removing the blobs outside the ROI on labeled PET image	60

LIST OF ABBREVIATIONS

PET	Positron Emission Tomography
CT	Computed Tomography
NSCLC	Non Small Cell Lung Cancer
SCLC	Small Cell Lung Cancer
FDG	F-Fluoro-Deoxy-Glucose
ROI	Region of Interest
ACS	American Cancer Society
NCI	National Cancer Institute
WHO	World Health Organization
CAD	Computer-Aided Detection
CHT	Circular Hough Transform
ISO	International Organization for Standardization

SUMMARY

Early and accurate diagnosis of lung cancer is one of the most investigated open challenges in the last decades. The diagnosis for this cancer type is usually lethal if not detected in early stages. For these reasons it is clear the need of creating an automated diagnostic tool that requires less time for the identification and do not require a cross-validation of the results by different radiologists, being in this way cheaper and less error prone. The aim of this work is to implement a completely automated pipeline that starting from the current imaging technologies, such as Computed Tomography (CT) and Positron Emission Tomography (PET), it will identify lung cancers to be employed for the staging; moreover, it will be a suitable starting point for a machine learning based classification procedure. In particular, this project proposes both a methodology and the related software tool that taking as input Digital Imaging and COmmunications in Medicine (DICOM[®]) files of chest PET and CT and by exploiting the characteristic of both of them is capable of automatically identify the lungs and the eventually presence of tumor lesions.

Going deeper into the topic and analyzing the literature it is possible to notice as very different solutions have been proposed in literature for an accurate and fast identification of lung cancer. Often such solutions start from CT and PT but generally they are semiautomatic tools that still require the intervention of a physician in charge of indicating which is the Region of Interest (ROI). On the other side, when fully automatic approaches has been proposed, they are closed source with not available datasets, so it is pretty impossible a comparison, as first, and

SUMMARY (continued)

to use their results to move forward machine learning based approaches. For this reason, this work proposes a methodology and its technical implementation that aim at being a reference point for future work into the field. As it will be possible to see, the thesis main contribution is about the proposition of a fully automated identification of the Region of Interest in the medical images, a fully automated segmentation procedure able to find lung cancer lesion inside the ROI and a technique for combine information obtained from both CT and PET.

A validation of the pipeline will be also discussed, measuring both the execution time and the obtained accuracy. Moreover, some consideration about future developments of this project will be proposed.

CHAPTER 1

INTRODUCTION AND MOTIVATION

The importance of early and accurate diagnosis of cancer is one of the most investigated open challenges in the last decades. For this reason, a high attention has been given to the creation of tools that can help physicians in this sense. In addition, among cancer types, lung cancer is the second leading death cause between both male and female after prostate and breast cancers [1], respectively. The diagnosis of this cancer type is usually lethal if not detected in early stages.

Cancer is a term that indicates a disease characterized by the uncontrolled division of abnormal cells that not only invade the tissues nearby, but also spread in term of metastases to other districts of the body through both blood and lymph systems [2]. Cancer can be classified with different names considering the starting location of the development and usually it is also described by a cardinal number that indicates the stage of progress of the disease [3]. The staging of lung cancer goes from one to four where one is an early stage cancer, while four is a terminal stage.

Considering that the 5-year survival rate for subjects with stage one lung cancer varies between 80-90%, while a late detection of this pathology can reduce the 5-year survival rate to less than 10% (stage four) it is crucial an early detection for increasing the possibility of survival. Within this context it is clear the need of creating an automatic diagnostic tool that requires

less time for the identification (compared to a physician) and does not require a cross-validation of the results by different radiologists, being in this way cheaper and less error prone.

Starting from the current imaging technologies, such as *Computed Tomography* (CT) and *Positron Emission Tomography* (PET), very different solutions have been proposed in literature for an accurate and fast identification of lung cancer. Most of them are based on a semi-automated protocol where the radiologist manually draws the Region Of Interest (ROI) and, after that, a program inside the decided ROI segments the tumor masses [4]. Such a choice can be useful in terms of reduction of diagnostic time, allowing the clinician to perform a first selection of the interesting part of the images, having then an identification made by a multi-step algorithm. The result can be further corrected by the physician if a over-segmentation or under-segmentation is performed by the semiautomatic tool. Semiautomatic tools are a starting point for speeding up the analysis process and a first step forward in the standardization of the obtained results due to the fact that they do not rely on human subjects for the entire procedure. On the other hand, they still require the intervention of the radiologist, who should manually select the Region of Interest slice by slice.

Following this trend, in the last years, some new fully automated identification tools have been proposed for the identification of cancer lesions in the lungs. Such tools rely on different characteristic of the medical images: for instance, some of them use approaches based on different stages of filtering and morphological operations [1], others on neural networks such as [5] and [6], some employ watershed techniques [7], and others prefer a graph based technique [8] and [9]. All these approaches can provide interesting possibilities in order to reduce the time

necessary for the identification of lesions, and most of the works affirm to reach a comparable accuracy considering as gold standard a cross-validated segmentation made by expert radiologists. In addition, a fully automated pipeline provides a standardization of the procedure reducing the interpersonal subjectivity between different physicians.

A further step for the reduction of the mortality rate due to lung cancer can be seen in machine learning approaches which, exploiting the information obtained from the segmentation, are able to provide information regarding the tumor. In fact, in recent years, attention has been given to these techniques for the classification of tumors. This type of analysis might be an interesting approach but, in order to produce reliable results, it needs a huge amount of data about physical and radiomic characteristics of the tumor masses [10]. For the collection of the aforementioned parameters it is necessary a standard segmentation method, otherwise the produced classification can be biased by the different calculation procedures [11]. Taking into account the necessity of congruence in the features extraction, an automated pipeline for the segmentation and the subsequently evaluation of the characteristics of interest proves to be a valid choice. As a matter of fact, it does not require the intervention of physicians assuring in this way the same method for the computation of the data for each analysis, overcoming in this way the problem of the human subjectivity. Moreover, considering the dimensions of the dataset, an automatic procedure will decrease the analysis time leaving to the radiologists more time for the treatment decision steps.

1.1 Thesis goal

For the aforementioned reasons the aim of this work is to implement a completely automated pipeline that aims at becoming the reference standard with the following goals: at first, it will identify lung cancer, secondly it will be employed for the clinical follow up; finally, it will be a suitable starting point for a machine learning based classification procedure.

For achieving these three objectives, this thesis proposes both a methodology and the related software tool that taking as input *Digital Imaging and COmmunications in Medicine* (DICOM) files of chest PET and CT and, by exploiting the characteristic of both of them, is capable of automatically identify the lungs and the possible presence of tumor lesions.

The proposed methodology lies on three main pillars:

1. An automated identification of the Region of Interest in the medical images;
2. An automated segmentation procedure able to find lung cancer lesion inside the ROI;
3. A techniques for combine information obtained from both CT and PET.

A validation of the pipeline will be done by computing the execution time, the reached accuracy and the visual results of the segmentation. The obtained accuracy varies between 89-97% on the analyzed dataset with a significant reduction of the analysis time.

1.2 Outline

Going next, Chapter 2 will give some useful knowledges to the reader about the physiological case study and about the imaging techniques employed for the data collection; Chapter 3 will discuss the state of the art, while Chapter 4 will states the faced problem and the goals of the

project. Continuing in Chapter 5 the details about the choices made for the data analysis will be presented. Chapter 6 depicts the details of the single stages of the pipeline; Chapter 7, then, will present the obtained experimental results and the comparison to the gold standard. Finally, Chapter 8 will draw the conclusions and possible future works starting from the achieved results.

CHAPTER 2

BACKGROUND

This Chapter presents to the reader some theoretical pillars in order to facilitate the understanding of the faced problematics and the proposed solutions. Section 2.1 presents a brief description of the anatomy of the respiratory system, while Section 2.2 describes the investigated pathology focusing on *Non Small Cell Lung Cancer* (NSCLC). Then, in Section 2.3 and all its subsections the imaging techniques employed for the data acquisition and their noteworthy characteristics are explained.

2.1 Respiratory apparatus anatomy

The respiratory system is a set of organs and structures that allows the gas exchanges between the alveoli and the outside environment. For the purpose of this work, particular attention is given to the lungs, which are the primary organs in the apparatus. The supportive tissue that composes the lungs is the parenchyma, which is made of elastic fibers. The lungs are positioned close to the backbone and on both side of the heart. As reported in [12], the space that divides the lungs containing the heart and other structures, such as trachea and esophagus, is called mediastinum. Moreover, the lungs differ one from the other for shape and size. In fact, the left one has two parts called lobes, as shown in Figure 1, and is smaller due to the presence of the heart, while the right one has three lobes and it is bigger.

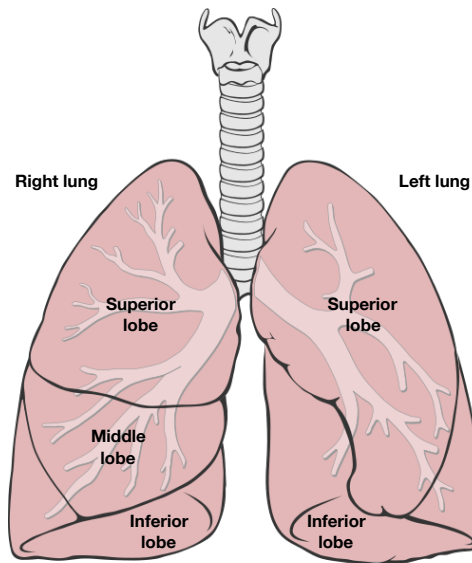


Figure 1: Diagram of lobes of the human lungs^{*}

^{*} Credits to Patrick J. Lynch; illustrator; C. Carl Jaffe; MD; cardiologist

Lungs have two main functions: ventilation and respiration. The former consists in the movement of air from inside the body to the external ambient and vice versa. The latter is essential for the wellbeing of humans and allows the gas exchanges [13].

The main task of the lungs is to supply oxygen to the body and to eliminate the produced wastes from the bloodstream. For doing so the lungs receive blood that contains very low concentration of oxygen from the tissues by the heart, while, through the pulmonary circulation, they eliminate the carbon dioxide produced by the body metabolism and provide oxygen to the blood, which then goes to the whole body [14].

Considering the fundamental functions of the lungs, it is clear that it is necessary a correct functionality of the system; however, some diseases can compromise them. In fact, lungs tissue

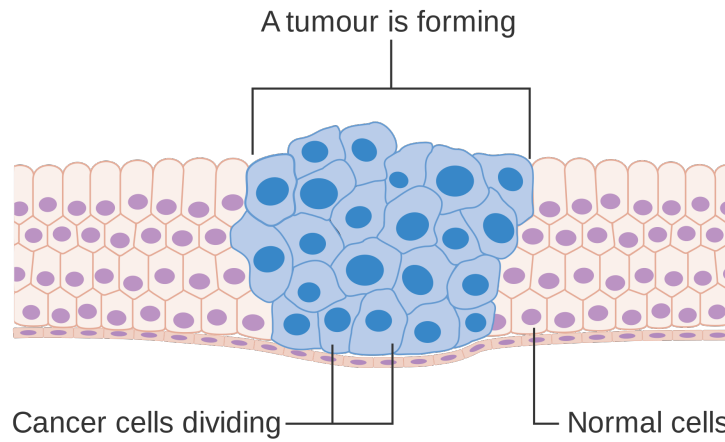


Figure 2: Representation of cancer cells spreading through healthy tissue*

* Credits to Cancer Research UK / Wikimedia Commons

may be affected by multiple pathologies such as pneumonia, chronic bronchitis and cancer [15]. Some of these diseases can be related or caused by smoking, inhalation of harmful particles or bacterias. In the specific case of this work the attention goes to lung cancer.

2.2 Investigated pathology

This Section will draw some trends and details about cancer and specially lung cancer in order to allow the reader to understand the importance of an early and correct detection of this disease.

As reported in [16], cancer is a pathology that is caused by an abnormal growth and division of malignant cells that create tumor masses, as shown in Figure 2. Moreover, some of these cells could spread into different body districts through the blood and lymph systems invading different tissues.

In a normal condition, cells follow a precise life cycle that is composed by different stages in which a newborn cell grows, duplicates and, at a certain point of its life, dies. The last step is called *apoptosis* and was firstly introduced by Kerr, Wyllie and Currie in [17]. Moreover, as reported in [18] it is part of the normal turnover of cells in fact, the old ones are replaced by new cells. On the other hand, when cancer appears, the normal life cycle fails in favor of an abnormal behavior where cells do not die when they should with a multiplication that is faster than normal. Within this context, humans affected by cancer show solid masses called tumor [19]. Tumors are classified as malignant or benign: benign tumors are masses that can reach huge dimensions but they do not move to different districts and, once removed, do not grow back again. On the other side, malignant ones can invade different tissues and potentially they can grow back once removed.

Lung cancer can be classified into two categories: Non Small Cell Lung Cancer (NSCLC) and Small Cell Lung Cancer (SCLC); the former is the most common one, while the latter is less common, consisting in around the 10-15% of the cases according to the American Cancer Society (ACS) [20]. In this work attention will be given to the NSCLC that can be further divided into subtypes such as adenocarcinoma which starts from the the glands and squamous cell carcinoma which starts from the skin that composes the airways [21].

Lung cancer is one of the leading causes of death in the world, even if it was quite rare at the beginning of the 20th century. Some suggests that increasing consumption of cigarettes is one of the reasons why this disease is more and more present. For century in the world, as said in [22], tobacco has been commonly used, but, in the present, cigarettes contain not only

tobacco, but also chemical additives and other potential harmful substances. During the 20th century, the rate of incidence of lung cancer has constantly increased from the 30's till reaching the maximum in the 50's when it has become the leading cause of death in men [23].

In addition to smoking some others are the identified causes of this increase in the occurrence of the pathology such as the air pollution, the diet and genetic inclination. In fact, as highlighted in [24] according to projection for the 2018 more than 1,700,000 new cases and more than half a million cancer deaths will occur in the United States. In the past decade according to the data collected by the American Cancer Society, the incidence rate of cancer was stable in women and was reduced by nearly 2% per year in men. More in detail, focusing only on lung cancer, the estimated number of new cases in the US will be around 230,000 cases nearly equally divided between male and female, while the projection about the deaths are around 150,000. Nowadays some step forwards have been done for reducing the death mortality rate. Prevention, treatments and early diagnosis, which is the scope of this thesis, have given the possibility to reach such great results.

Considering the general five year (2007-2013) relative survival rate for lung cancer at all stages in the US was around 18% according to [24], so taking into account the aforementioned data it is quite clear the necessity to an early and accurate identification of tumor lesions. The possibility of an early diagnosis can provide the opportunity to choose the most appropriate therapy increasing the survival rate.

2.3 Imaging techniques

In the medical field the identification of pathologies in the early stages is a crucial open problem that is at the base of a correct diagnosis and a subsequent decision of the most appropriate therapy. An invasive method for lung cancer detection is the employment of biopsy, which is an extraction of a tissue sample from the living patient [25]. It is clear that this approach is painful for the subject since it involves surgery. In order to avoid or reduce the employment of this dangerous technique some alternatives have been proposed, such as imaging based assessment. For example, in the past, one of the most used technologies was the X-rays imaging [26], while in recent years it has been used the F-fluoro-deoxy-glucose Positron Emission Tomography/Computed Tomography imaging method, known also as FDG PET/CT. This examination allows the fusion of information from multiple sources giving, in this way, a more precise and accurate reproduction of the inside of the human body. Next Sections describe more in detail both the CT and the PET.

2.3.1 Computed Tomography

The Computed Tomography (CT) is a clinical imaging technique that exploits a X-rays beam in order to acquire signals, that after being elaborated by a computer, generate images generally called slices. The images are spatial representation of the attenuation coefficient of the rays in a section of the scanned object and can be considered as tomographic reconstructions of the body that contain more information compared to the traditional X-rays. The obtained images can also be stacked in order to form a 3-D reconstruction of the body district investigated, facilitating the visualization and the identification of organs or abnormal structures by a specialist [27].

The main difference between the conventional X-rays and the CT is that the first one uses a fixed source, while the CT has multiple sources that rotate around the patient inside a circular structure called *gantry*. A CT scan is a clinical examination that consists of a collection of multiple contiguous images of a specific part of the body in accordance to the area of interest of the clinician, as shown in Figure 3. During the acquisition, the patient lies supine on a table, that can be moved in or out of the gantry while the X-rays sources rotate around the subject [28]. The sources constantly release beams of X-rays that, passing through the human body and reaching digital detectors, which are positioned opposite to the sources, are able to create the images.

The creation of a single 2-D slice is possible only after a complete rotation of the sources. In fact, in order to reconstruct the image, it is necessary to apply to the signals collected a mathematical procedure called *back-projection reconstruction* [29]. This step is done through the *Radon transform*, which, considering the angle of acquisition of each signal, is capable of mixing them in the most suitable way for reducing the creation of artifacts. This procedure is repeated for each movement of the table so that the entire region of interest is covered. The thickness of each slice can be decided by the physician, but it usually varies between 1 to 10 millimeters and the dimensions of each pixel are around few millimeters, allowing a very good spatial resolution [30]. Due to this intrinsic geometric characteristics, the CT is often preferred to the X-rays and has become a common tool for the identification of lesions and tumors in the abdomen, lungs, head and also for inspection of the heart [31]. Consisting in the same technology of the X-ray, the CT can easily discriminate between hard and soft tissues due to

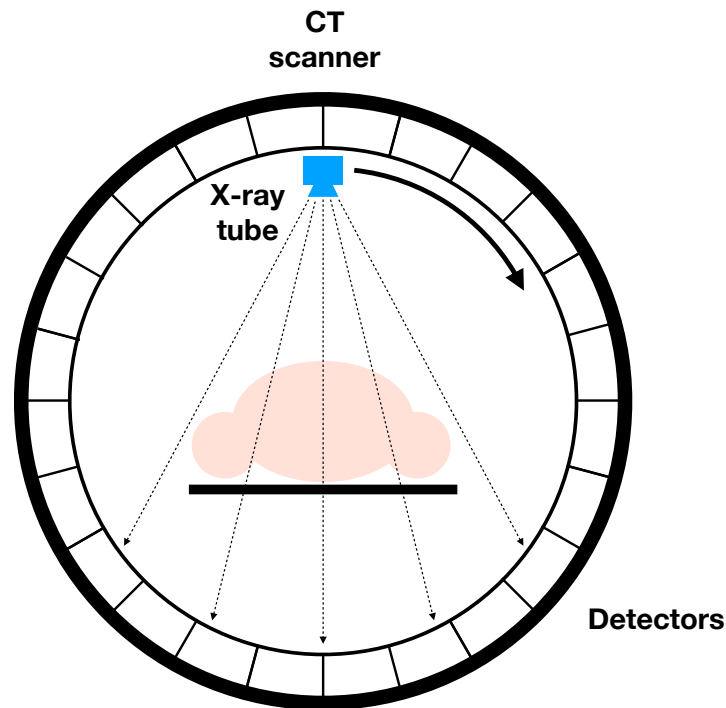


Figure 3: Basic scheme of Computed Tomography

the fact that structures such as bones stop the rays creating light spot in the image, while soft organs result in darker shape in the reconstructed image. For the aforementioned reasons, the CT is a good standard for structural investigation; however, Positron Emission Tomography, which gives details about the metabolic active structures, allows a more precise identification of tumors.

2.3.2 Positron Emission Tomography

The Positron Emission Tomography (PET) is an imaging technology used in nuclear medicine that allows the assessment of structures functionalities employing radioactive substances. The

PET creates 3-D images using radio-pharmaceuticals as tracers, which decay releasing positrons, which are then used for the creation of the images [32]. Positrons are particles that have similar mass to the one of electrons but with opposite charge, so passing through the human body they combine with the electrons and annihilate one another. This chemical reaction releases energy and two photons which produce two γ rays that, as shown in Figure 4, are shot in opposite direction and by colliding with the detectors are employed for the creation of the acquired images [33]. The main limitation of the PET is that it has an intrinsic low spatial resolution mainly due to the physical width of the detectors in combination with the decoding of the signal and the penetration. In fact, as highlighted in [34], if the γ rays are not perfectly perpendicular incident onto the detectors, they can interact with more than one detector so the signal can be associated to the wrong one degrading the resolution of the final image.

The tracers used for a PET scan are formed by carrier molecules bonded to radioactive atoms and usually are administrated to the patient by injection, inhalation or ingestion [35]. The total amount of the tracer is so low that it does not influence the normal function of the system: for these reasons the PET is defined as physiologic tomography. This methodology is based on the emission of positrons β^+ from the decay of the isotopes, which have a very short life, so, after a short path, (for example in lungs where there is the lowest tissue density), these positrons can reach maximum few millimeters. In the tissues, positrons annihilate with a negative electron generating in this way two γ rays of 511 KeV (Kilo electron Volt) emitted in opposite directions (180°) [33]. Positioning a couple of detectors is possible to exactly identify the line along which positrons have been emitted, shown in Figure 4. In addition, if two logic

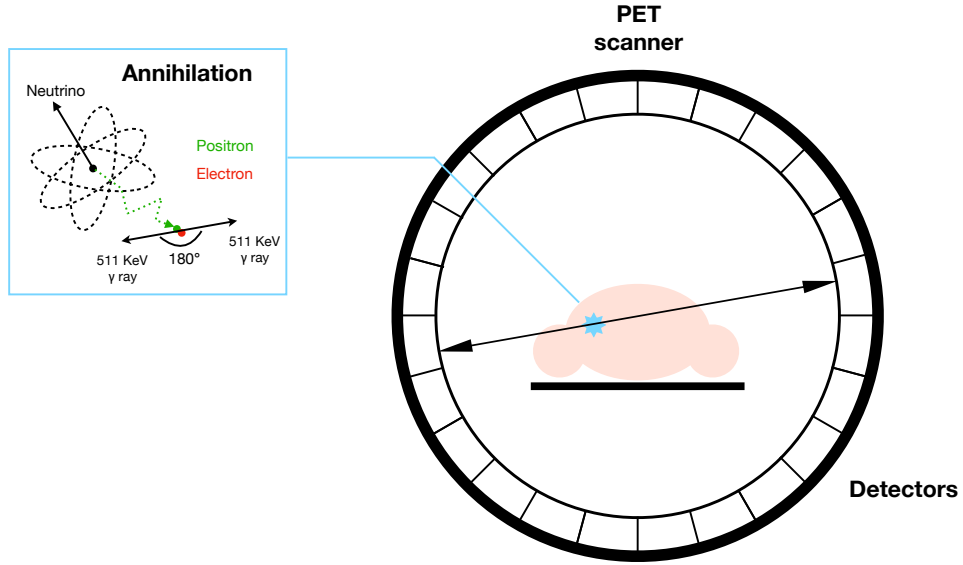


Figure 4: Basic scheme of Positron Emission Tomography

impulses are super imposed in time, the system recognizes an annihilation and records also the integral value of the line joining the two activated crystals, which is then coded in the image.

The aim of PET imaging technique is to identify cancer, monitor it and verify the efficiency of treatments, in addition to the detection of metastases. As tracer is usually used glucose because cells or tissues that have a high metabolic activity, such as dividing cancer cells, request a huge amount of energy, which means an increase in the glucose consumption. In fact, the more the cancer is aggressive, the more rapidly it will utilize glucose. For these motivation radiolabeled glucose is employed as tracer for the detection of cancer and metastases spread in the body [36]. In the proposed work the tracer used for the PET acquisition is F-fluoro-deoxy-glucose (FDG).

Summarizing what has been said above it is possible to conclude that the CT provides images with a good spatial resolution giving interesting details about geometry and mechanical properties of the internal structures. On the other hand, the PET, which lacks in spatial resolution, is able to highlight the metabolic active areas allowing the identification of the structures that are requesting a considerable amount of blood such as the heart or tumors. As confirmed by [37] scanning the same body district with both in one examination (PET/CT imaging) has become a highly employed tool for the identification and the staging of cancer all around the world thanks to the combination of anatomical (CT) and functional (PET) information. For the aforementioned reason, this thesis employs data acquired by the FDG-PET/CT, in this way, the proposed pipeline is able not only to analyze the selected dataset, but also other dataset acquired with this widespread technology.

CHAPTER 3

RELATED WORK

As described in the previous Chapters, the detection of lung cancer is a challenging process and it can be faced in different ways, so this Chapter presents a review of the State of the Art of the employed methodologies. The currently available approaches can be divided into two main groups: the first one uses surgical and invasive tests, such as biopsy, while the other includes all the non invasive techniques based on the medical imaging. A further classification inside the second group can be done on the basis of the chosen method for the identification of the tumor masses. Following this separation, Section 3.1 will explain the differences between an invasive and a non-invasive technique for the assessment of the pathology. Subsequently, focusing only on the imaging, Section 3.2 will describe the details about the possible choices to be done for segmenting the cancer lesions, while Section 3.3 will present the difficulties to obtain open sources datasets (due to privacy constraints) for validating the works proposed in the State of the Art.

3.1 Invasive vs non-invasive assessment techniques

The gold standard for lung cancer identification through the decades have been changed several time according to the step forward done in the technology development, moving from more invasive tests to non-invasive approaches based on imaging techniques.

In the past, for lung cancer detection, chest radiography and sputum cytology were employed as reported by Hirsch et al. [38] due to a trial sponsored by the National Cancer Institute (NCI) that in the 70's was held at the John Hopkins University, the Mayo Clinic and the Memorial Sloan-Kettering Cancer Center [39], [40] and [41]. As confirmed by the authors, this trial however failed to demonstrate the decrease of the mortality rate by employing the aforementioned exams. A further step was done according to the World Health Organization (WHO) employing light microscopy with hematoxylin and eosin on a sample of tissue [42]. This procedure is invasive due to the necessity of a specimen of the possible tumor. Then in the WHO classification of 1999 was introduced the immunochemistry and, until 2004, it was used only for a small class of cancers types due to its invasiveness. Nowadays, biopsy is still used in the medical practice but, usually, after a first screening done by a non-invasive technique and as a post surgery assessment on the removed masses for extracting useful information about the characteristic of the tumor.

One of the first non-invasive tests employed in the clinical field for the screening, identification and staging of the lung cancer was the X-ray imaging. This procedure is considered non-invasive, even though the patient is subjected to a beam of rays that passes through the body (usually low dose less than 10 milliGray) [43], compared to collection of a sample of tissue, it greatly reduces the discomfort and the risks for the patient. X-rays, as defined by [26], are a radiation that can be employed both as an imaging technique in diagnosis and as a treatment for cancer. From the X-rays, the technology has moved forward in order to overcome some limitations of them, such as the impossibility to obtain a 3-D reconstruction of the area of

interest of the human body; indeed, since the acquisition is done from a single angle, it is not possible to generate a 3-D reconstruction. The X-rays produce a 2-D image representing the coefficient of attenuation of the beam passing through different types of tissues, for instance bones and soft tissues. The differences in the mechanical properties of the biological tissues are reflected in the pixel intensity in the final image corresponding to that particular tissue.

As a result of the technological progress, *Computed Tomography* (CT) and *Positron Emission Tomography* (PET) are nowadays within the most employed imaging techniques for the screening and the identification of multiple pathologies, including lung cancer. As previously explained in Section 2.3, medical imaging is a field in continuous development to increase the employment of non-invasive techniques in diagnosis. For the screenings or detection of tumor masses, the use of these techniques can reduce the stress for the patient avoiding a surgical intervention and its risks. Moreover, imaging can be used as a preclinical tool for the decision-making process for the most suitable treatment without the necessity of directly intervene in an invasive way.

CT and PET can be used separately but more and more frequently are jointed to combine information both from a structural and a functional point of view. In fact, as previewed in Section 2.3.1, the CT has a good spatial resolution giving the possibility to highlight the details of the inside of the body district investigated. The good resolution allows a discrimination between the bones, the air inside the body and soft tissues; this classification is done exploiting the density of each structure, where a dense one appears lighter on the resulting image, while a hollow results as black. Considering the aforementioned characteristics the CT can be used

for obtaining anatomical details that are useful for the identification of multiple diseases but cannot be enough when detailed functional information are needed. PET, on the other hand, as said in Section 2.3.2, thanks to the used radio-tracers, provides information about the metabolic activity of tissues. In fact, more active is the structure, more metabolic request it has and more blood containing the tracer it beckons resulting in a bright spot on the image.

3.2 Segmentation methods

From previous works, non-invasive techniques seem to be the most promising approaches for the study of lung cancer and the FDG-PET/CT, as chosen imaging technique, exploited for the image acquisition, it is now possible to present the different techniques for the identification of the cancer lesions.

A first discrimination can be done between *semi-automatic* and *fully-automatic* approaches: the first one requires the intervention of a human being at least for the decision making step, which consists in the identification of the Region of Interest (i.e. part inside the lungs containing the possible tumor); the second one, starting from the input dataset, is able to automatically identify the tumors without any additional information or manual intervention. Being the aim of this work to implement a fully automatic pipeline, all the works which present a semiautomatic implementation will be not considered.

3.2.1 Neural Networks

Nowadays, more and more image processing methods for the recognition of tumors are based on *Neural Networks* (NN), a computing system able to learn from an input dataset how to recognize patterns or structures on the one side, or to classify the images on the other. The

learning process consists in the elaboration of a training dataset that must have considerable dimensions in order to generate an accurate network [44]. The output of the training phase is a trained network that can therefore be employed for the recognition of objects within the image or for their classification.

Unfortunately, due to the necessity of a training dataset with high cardinality, this kind of approach is hard to be implemented for the classification of lung cancer, since, generally, on the one side, open source datasets have limited dimensions and, on the other, the creation of a useful dataset with a sufficient number of patients is expensive both in terms of time and costs. Moreover, working in medical field, there are privacy issues that can slow down the creation of such datasets.

However, Neural Networks are widely used in non-medical fields for image processing purposes, due to their accuracy in the classification when correctly trained. Currently, biomedical research is moving toward the usage of such methods in diagnostic field exploiting the knowledge already acquired in other research fields to obtain advancements on medical applications [5]. Generally, state of the art works such as [45] tend to validate the proposed methodology on synthetic images or by performing a data augmentation (i.e., the generation of new data from existing ones using synthetic techniques like image rotation, filtering, etc...) in order to create a sufficiently big dataset [46]. However, even if a testing on synthetic data might be a good starting point, it is still necessary a validation on a real case study in order to employ the obtained network on the actual medical field.

3.2.2 Watershed algorithm

A second approach proposed in literature is the employment of watershed segmentation methods that are used to identify the contours of regions containing local minimums [47], [48]: however, as reported by the authors, in order to reach a good efficacy, some object markers (starting point positioned in specific position on the image) are needed. Unfortunately, the decision of their correct position on the image, depends on some a-priori knowledge like the number of objects, some specific feature or the object locations [49]. Such requirement leads to the impossibility of the usage of such method for an automatic segmentation: in fact, the necessity to have as input these data is strictly related to the intervention of a human being. Moreover, also a low image contrast can bias the result obtained by watershed approaches. In fact, such method is based on the water basins division theories born within the geological field. Based on this theory, the image segmentation is done by considering light spots as hills and the dark ones as valleys, and thanks to a virtually flooding of the image the separation of the different regions may be done [50]. At this point, the water flows from the hill to the valley till, reaching the minimum: the segmented areas are the one containing the water flooded till the minimum (basins). It is then clear that a wrong image contrast can lead to wrong results.

3.2.3 Graph-based approach

Also a graph-based approach can be employed for the segmentation of the tumors, as explained in [51]. In fact, it is possible to start from a random walk procedure to attribute a specific label to unknown nodes [52], both on connected (for each couple of nodes there is at least one connecting edge) and undirected (all the edges are bidirectional) graphs. The sub-

sequent segmentation is done thanks to the cut edge technique that has proven to produce good results as in [51]. However, such approach lacks of scalability since it rapidly increases in memory usage during the computing process with respect to the increment of the image size [53].

3.2.4 Morphologic and filtering approach

Last but not least, due to their low budget development, the most commonly used approaches are based on morphological information and on the filtering of the obtained images [54]. Such approaches are generally convenient since they exploit characteristic of the images themselves, without requiring any wide dataset for the training process, thus reducing costs [4]. For the aforementioned reasons, in the last decades, the image processing approaches based on filtering and morphological operations have been employed and widely developed in multiple research field. This widespread employment has allowed a rapid and efficient development of multiple techniques that combined together have proven to be a valid and low cost method for image processing and segmentation [55].

3.3 Data availability and evaluation challenges

This Section will draw some considerations about the data availability and, more details, about the evaluation approaches available in literature for the segmentation results will be explained.

The first important step to start an image processing project is the image retrieval: here, some difficulties can be faced since, on the one hand, there are huge privacy issues (anonymous image should be employed), while, on the other, being the image taken from human subjects,

rarely the datasets employed in the literature are available and open source. Moreover, also when such datasets are accessible, they do not contain the annotation done by an expert radiologist, making them not usable during the validation part of a new discovered method. For these reasons, the majority of the works employ private datasets created by specialist research institutes where the radiologist can manually analyze the images and compare the obtained segmentation with the one obtained automatically.

An additional problem, which is reflected in the lack of standardization in the obtained results, is that only few works propose a quantitative analysis of the results, while most of them graphically compare the automatic results with the manually segmented region. Moreover, results are generally about the tumor classification, while it is hard to find results about the segmentation, since it is done at the first step of the processing pipeline.

3.4 Summary

Within this Section a brief summary of the decisions made for the development of this project will be proposed focusing on the identification method and the validation of the final results.

For which concern the cancer identification, the proposed tool will rely on morphological and filter-based algorithms to obtain an accurate pipeline that can produce standard results for different types of acquisition techniques and a low dataset cardinality. Differently from the State of the Art solution, the proposed work aims at being a reference point providing all the possible data to experimentally replicate the solution. Moreover, differently from the existing

works, this thesis proposes a fully automatic and systematic approach to analyze both the PET and CT together in order to find complex tumor masses.

Considering the validation step, it is complex to validate the obtained results for two main reasons: on the one hand, if the description of the algorithm is detailed, generally the dataset is not available; on the other hand, if the employed dataset is open source, the details about the employed pipeline is not reproducible. For these reasons, the most commonly employed validation is the one based on a comparison with the manual segmentation. Moreover, there are only few works that provide quantitative statistics on the obtained results and the source code of the implemented pipeline. Both these two factors make impossible a direct comparison of the obtained results. Considering what has been said, it is easy to understand that there is the need to standardize both the procedure of the dataset creation and more important the results evaluation. This is what this work aims at providing: a first attempt to give comparable results for other future studies.

CHAPTER 4

PROBLEM STATEMENT AND GOALS

The aim of the following Chapter is to describe the decision making process behind the choice of the faced problem and to explain which are the goals of the proposed work in relation to the field of application. For this reason, Section 4.1 describes the motivations which led to the formulation of the proposed project, which has been conceived in collaboration with a medical research group who shared their real life experiences. Starting from their inputs and knowledge, a systematic analysis of the currently employed technique has been done in addition to the study of the existing approaches in literature (see Chapter 3). Then, the goals of the proposed work have been set to fulfill the requests of the physicians: Section 4.2 explains these objectives in detail.

4.1 Problem definition

This Section presents the assessed problematics that have been chosen thanks to a discussion done with a medical research group that is working for the creation of a standard and accurate methodology for the identification and the classification of lung cancer. The most important problems that have been highlighted are:

1. the necessity to identify the cancer lesions in an automatic way to obtain a reduction of the diagnostic time allowing radiologists to interpret the final results, instead of analyzing each image and drawing manually the contour of the tumors.

2. the necessity to produce a tool that can be a reliable starting point for further analysis, such as the extraction of geometric and radiomic features that can be later on employed for a classification procedure.

The discussion had with the medical research group are supported also by some works already present in literature; in fact, even though imaging approaches to the problem of early lung cancer identification are relatively new, some works have been proposed in the last ten years. As said before (Section 3.1), considering only the non-invasive approaches as starting point for the data collection, some elderly works based their identification of cancer lesions only on the CT images; however, even if this can be a good starting point, they have many issues in the computation of the segmentation since they do not take into account any metabolic activity. For this reason, as already introduced, the data that will be employed in the proposed thesis are obtained by two subsequently acquisitions: CT and PET.

Summarizing, it is possible to say that the presented work will stay within the trend of providing a computer based approach for the study of lung cancer since this can lead to make steps forward into the study of the pathology for early diagnosis and to obtain more effective therapies.

4.2 Thesis objective

In order to fulfill the request done by the physicians and to move forward an accurate detection of lung cancer in early stages, the aim of this work is to propose a methodology and the correlated software tool that, exploiting the data obtained by one of the most common clinical exams in this field (FDG-PET/CT), is able to properly identify the contour of the

tumor lesion, limiting the possible false negative (lung cancer patients identified as healthy) and reducing the total diagnostic time. It is important to consider that the employment of that specific type of images is done considering the spreading of this imaging technique within the cancer detection field [56].

Within this context, the objective of this thesis is to create a tool able to load images obtained from the machinery and thanks to multiple filtering steps and the exploitation of morphological features of the images themselves (later explained in Chapter 5 and Chapter 6), needs to be able to select the contour of the tumors and to provide as a result the input image where the identified boundaries are drawn in white. Radiologists and physician expressed the request to have a tool able to perform a visual rendering, since it is easier for them to perform further analysis. For this reason, an important goal is to keep the same data format of the input images as output.

Another request coming from the medical research group was the possibility to have a completely automatic tool: this request relies on the needs of speeding up the computation while assuring also the same accuracy and execution time for each single image analyzed. In fact, on the contrary, the performance of a radiologist can vary with respect to the number of worked hours and multiple external conditions (i.e. tiredness, distractions, etc.). For these reasons, as explained also by the authors in [57], the employment of *Computer-Aided Detection* (CAD) tools is really important in the medical research field.

A final goal of the proposed work is to has the objective of providing an accurate and easy to use tool that will also facilitate the creation of a standard procedure for the early identification

of lung cancer allowing a further extraction of features for a subsequently classification done by machine learning approaches.

CHAPTER 5

METHODOLOGY

This Chapter gives a detailed description of the proposed methodology to the reader to better understand the choices that have been done for each of the preprocessing and processing steps. In Section 5.1 a brief introduction to the entire work-flow is described; Section 5.2 gives the composition of the dataset highlighting the differences between the images taken from the CT and the ones taken from the PET. Continuing in Section 5.3 the description of the preprocessing steps is provided, while Section 5.4 presents the procedure employed for the segmentation of the ROI on the CT images. Then, Section 5.5 explains the analysis of the PET images. Finally, Section 5.6 shows the union of the data obtained from both sources and the final identification of the tumor contour.

5.1 Proposed pipeline overview

In order to explain the single processing steps implemented for obtaining the most accurate segmentation possible, it is useful to start from a description of the overall methodology, allowing the reader to have comprehensive idea. Figure 5 shows the overall work-flow scheme highlighting how can be divided into two different parts: one related to the CT and one to the PET. The results of the two calculation is then merged for achieving the wanted segmentation.

The CT branch is composed by a preprocessing phase and a processing one. The former aims at deleting the possible artifacts given by the gantry (cylinder shaped scanner employed

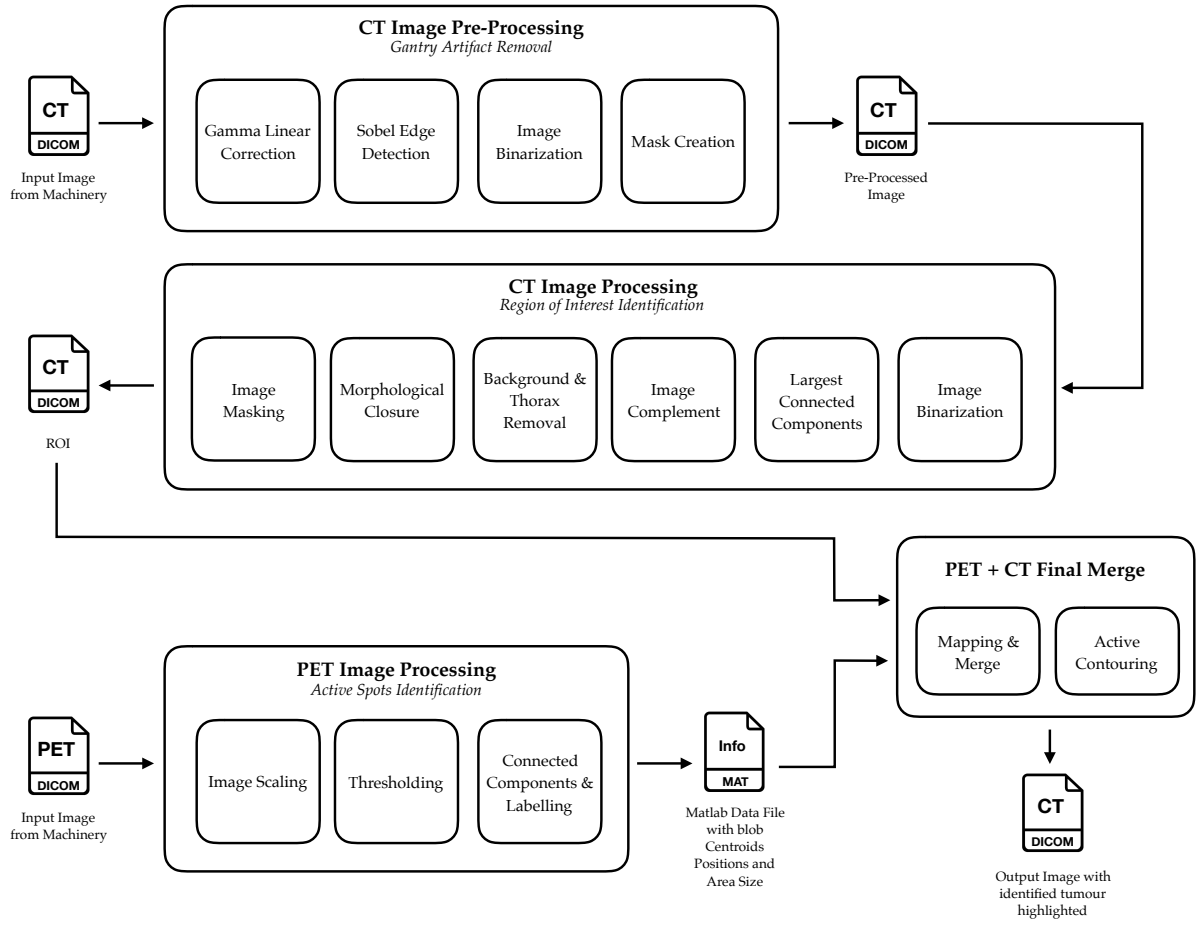


Figure 5: Scheme of the implemented pipeline

for medical imaging [58]), while the latter, starting from the identification of the lungs, is then able to highlight the details such as tumors and small bronchioles. This step is fundamental for selecting the areas where the tumors can be present reducing, in this way, the false positives (i.e. parts identified as tumors when they are not).

The PET phase, on the other hand, is able to select the areas that are active which coincide with the lighter spots in the image. By finding the centroid of these structures, it is possible to identify their location in a reference system that can be further used for reporting them on the CT.

In the end, as anticipated before the locations of the active spots in the PET are reported on the CT, where the centroids outside the lungs are discarded, while the ones inside the lungs and overlapped to an interesting areas (e.g. bronchioles or tumors) in the CT are kept. The points that have passed this test are used as seeds for the identification of the areas that contain them, finding in this way the contour of the tumors, which are usually round shaped and metabolic active if compared to the linear and not active shape of the bronchioles.

5.2 Dataset description

As already introduced in Section 2.3 the employed images are: CT and PET; both of them are *Digital Imaging and COmmunications in Medicine* (DICOM) format, which is the one usually employed as a standard in the medical imaging field [59]. For each patient, the number of images can vary according to the dimensions of the acquired anatomical district. This variable is decided by the radiologist and can be influenced by the height of the patient. In fact, a taller patient needs more slices to cover the entire lungs if compared to a shorter one. Moreover, the dimensions of the lungs can vary between genders. For these reasons the total number of images cannot be standardized but depends on different factors. Within this work, for all the patients both the CT and the PET stacks start from the nape until the pelvis. In addition, the acquisition can be standard or helical. The former is a step by step acquisition

where the machinery scans one portion of the body before moving forward to scan the adjacent one without any overlapping areas. On the other side, the latter has a continuous scanning all over the body thanks to a helical movement of the gantry. As a consequence, an overlap between adjacent slices appears.

The thickness of the slice can vary between the standard and the helical mode. Moreover, for the helical images the overlap between subsequent slices is generally around 13% leading to an higher number of collected slices if compared to the standard acquisition. The decision of the acquisition protocol is done by the physician according to the model and the brand of the machinery. In this work, both the options are considered and handled in order not to limit the use of this methodology with respect to the features of the medical device.

For what concerns the PET images, in accordance to what has been said for the CT, the acquisition can be as well standard or helical, but, in this case, the difference is not only related to the thickness of each slice and the overlap, but it is also related to the dimensions of the single image. In fact, if the acquisition is standard, the image will be smaller if compared to the helical one. Moreover, as said before, the thickness of the slice varies from the two protocols. The standard acquisition of the PET has a thickness of half of the thickness of the standard CT, while the helical one has the same thickness of the CT. Also this difference of dimensions and thickness, will be taken into account for the mapping of the PET information on the CT mask, in order not to introduce distortion in the information during this process.

5.3 CT preprocessing

The first step in every image processing work is the preprocessing; such step has the scope of normalizing the input and modifying some details to allow a better extraction of the wanted details. In this Section the focus will be on the steps employed for the preparation of the CT. Since the dataset is composed of two different categories of images (standard and helical, see Section 5.2), there are some normalizations to be performed. In fact, the helical acquisition produces the gantry artifact on the image, resulting in the presence on the image of a circular shadow around the patient’s body. This is due to the shape of the cylinder where the patient is inserted and, if it is not removed, it causes a wrong segmentation of the lungs.

For the removal of this artifact, two different strategies can be employed: the first one exploits the meta-data that are available within the DICOM images, while the second one works directly on the image itself. The decision of the more suitable approach is subjected to the comprehension of the differences between them and to the kinds of information that are needed by both of them. The approach based on the meta-data can be useful because it does not require any additional image computation to detect the gantry artifacts; however, it is not always applicable, since it depends on the presence of the field of the “ScanOptions” in the meta-data structure, as shown in Algorithm 1. If the field is reported in the meta-data it is necessary to read if the acquisition mode is helical, if this condition is verified it is possible to start with the preprocessing steps, while if it is not helical it is necessary to skip all these steps starting directly with the segmentation of the lungs procedure. On the other hand, if the meta-data are not considered, it is still possible to identify and remove the artifact.

Data: input CT image
Result: acquisition method
 info \leftarrow CT meta-data;
 option \leftarrow isfield(info, 'ScanOptions');
if option **then**
 | helical acquisition;
else
 | not helical acquisition;
end

Algorithm 1: Pseudocode of the CT acquisition method

In order to handle a more generic scenario, in the proposed work, the second approach has been implemented, due to the fact that sometimes the “ScanOptions” field in the meta-data can be omitted. The first step of the preprocessing consists of an adjustment of the acquired image in order to increase the contrast. This step is done in order to make the circular shadow more visible facilitating in this way the subsequent identification and removal. The adjustment has been done by a linear gamma correction algorithm ($\gamma = 1$), which maps the gray values of the input image into new ones in the output image and it saturates both the top and the bottom 1% of all pixel values.

Thanks to the contrast enhancement, the second step can be performed: an edge detection. Given the input image, it creates a binary image where a value of 1 corresponds to an edge, while the remaining parts are all zeros. The chosen method for the edge detection is the Sobel algorithm [60], which identifies as belonging to an edge those pixels where the gradient of the input image is maximum. This edge detection algorithm therefore implements the Sobel approximation of the derivative function with a 3x3 kernel. The formal representation of the

kernels are report below in Equation 5.1, while Equation 5.2 and Equation 5.3 report respectively the formula of the magnitude and the direction of the gradient.

$$S_x = \begin{bmatrix} 1 & 0 & -1 \\ 2 & 0 & -2 \\ 1 & 0 & -1 \end{bmatrix} \quad S_y = \begin{bmatrix} 1 & 2 & 1 \\ 0 & 0 & 0 \\ -1 & -2 & -1 \end{bmatrix} \quad (5.1)$$

$$G = \sqrt{G_x^2 + G_y^2} \quad \text{where} \quad G_x = S_x * Im \quad \text{and} \quad G_y = S_y * Im \quad (5.2)$$

$$\Theta = atan \left(\frac{G_y}{G_x} \right) \quad (5.3)$$

Another fundamental step for the removal of the artifact is the binarization of the original CT image: a new image where what is contained in the circular shadow is set to white (while the outside background is set to black) is obtained. The binarization is based on the global threshold using the Otsu's method [61]. As reported in Algorithm 2, the optimal threshold value is selected and then used for binarizing the image. This method computes the threshold based on the minimization of the intraclass variance (combined spread) of white and black pixels; such threshold is then compared with the value of each pixel of the input image and, if the pixel value is higher than the threshold, it is set to white, otherwise is set to black.

Having binarized the CT image it is now possible to identify the circumference presence by employing the *Circular Hough Transform* (CHT). This transform is a features extraction

Data: input CT image
Result: binarization threshold
 histogram and probabilities of intensity levels;
 $\omega_i(0) \leftarrow$ initial probability;
 $\mu_i(0) \leftarrow$ initial standard deviation;
for $t=1, \dots, \text{max_intensity}$ **do**
 $\omega_i \leftarrow$ update probability;
 $\mu_i \leftarrow$ update standard deviation;
 $\sigma^2(t) \leftarrow$ computed variance;
end
 $T \leftarrow$ threshold correspond to max of $\sigma^2(t)$
Algorithm 2: Pseudocode for the Otsu's method

procedure that is able to detect circumferences inside an image; in other words, it is able to finds circles in the image that have a radius in a certain range.

Given the circumference expression in Equation 5.4 where (a, b) is the location of the center of the circle and r the radius, as said in [62], it is possible to find the center if a (x, y) pixel is fixed and the radius is known. However, if the radius is not known but, as in the considered case, it is contained in a certain fixed range, the computation should be iterated through all possible radii.

$$(x - a)^2 + (y - b)^2 = r^2 \quad (5.4)$$

Obtained the contour of the original CT thanks to the employment of the edge detection algorithm and of the binarization, it is now possible to perform the absolute difference between them. This step is performed to obtain the mask that will be used for filtering the CT and

removing the gantry artifact. The value assigned to each pixel of the output image is given by the difference between the corresponding pixels in both the result of the edge detection procedure and the binarized image.

Finally, the original CT image is filtered with the previously created mask, allowing the elimination of the circular shadow and leaving unmodified the remaining objects in the image. This procedure consists in a multiplication element by element of the CT with the mask.

5.4 Lungs segmentation

After the preprocessing on the CT images, it is now possible to focus on the segmentation task, thanks to which it will be possible to preserve only the lungs structure and removing all the other parts such as the table where the patient lies, the arms, and the ribcage. As introduced in Section 5.3, the starting point for the segmentation can be either the original CT, if the gantry artifact was not present, or the preprocessed one. For the segmentation purposes the applied steps are the same in both conditions and will be described shortly.

The first step of the segmentation procedure consists of the image binarization with the threshold chosen with the Otsu's method previously explained in Section 5.3. After that, it is necessary to remove the table where the patient lies, because in further steps the presence of the table will prevent the identification of the lungs. A simple approach can be chosen for this purpose: setting as background (black) the lower part of the image, interrupting the continuity of the table borders. By having interrupted the contour of the object, it assures the fact that in a further processing step it will not be recognized as a structure of interest.

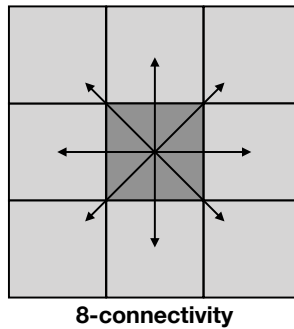


Figure 6: 8-connectivity representation

In fact, on the binarized image is then possible to remove the table and the patient's arms by keeping only the biggest connected components. For doing so it is necessary to decide the connectivity value that, in the faced case, is equal to eight, as suggested in [63], which means that, to decide if a certain pixel is part of the connected components, the eight pixels adjacent are considered, as shown in Figure 6.

After the attribution of every pixel of the image to a structure (labeling process), a certain number of components will be found and, in order to keep only the thorax, which is the one containing the lungs, is necessary to sort the found objects based on the area dimension. By selecting the biggest one, the arms and the table are removed, obtaining as result an output binary image where the inside of the lungs is black as the background, while only the shape of the thorax is white. In order to extract not only the shape of the lungs but also the detail of the structures that they contain, such as the bronchioles and possible tumors, further steps should be implemented.

Keeping in mind that the region of interest should be identified as foreground and, from the previous step, the lungs were set as background, it is necessary to complement the previously obtained image. By doing so the white pixels become black and vice versa, so that the output is an image where what was the background and the inside of the lungs are light, while the ribcage has been set as background.

In order to create the mask that will be used for segmenting the lungs and their inside, the image should have only the shape of the lungs white with all the rest set to black. In order to do so, there is the need to reset the background from white to black thanks to an algorithm that allows the clearing of the borders. In this way, it is possible to suppress structures that are connected to the image border and that are lighter, if compared to the adjacent pixels. The explained approach is able to remove all the white pixels outside the thorax of the patient, which is considered as the border of the ROI to be segmented. At this point, the output image is close to the one that will be employed for the filtering, but there are still small unwanted black details inside the lungs, which should be removed to preserve, in further processing steps, the investigated details.

In order to remove the small objects inside the lungs in the created mask, a morphological close operation has been applied. This procedure is composed by two steps that are a dilation followed by an erosion, and both of them are performed by the employment of the same structuring element. In the analyzed case, the structuring element is a 2-D binary valued neighborhood, where the true pixels are used for the morphological computation, while the false ones are not. The employed structuring element is a round shaped neighborhood that, for speeding up the

computation, has been approximated with structuring lines (polygon approximation). As said, the first step is the dilation, which uses the selected structuring element for probing the input image and expanding the objects in it contained [64]. Finally, the erosion is performed; this operation is the dual of the dilation process and, for this reason, it can be seen as a shrinkage process that, using the structuring element, probes the input image and reduces the objects in it contained [65]. At this point, all the small details inside the lungs are removed leaving as the only white object in the mask the empty shape of the lungs.

Having obtained the mask it is now possible to filter the the CT and segment in this way the lungs maintaining all the information inside of them. The masking, as said in the last step of Section 5.3, is a multiplication element by element between the CT and the mask. At this point the desired result has been reached and can be saved and employed for the fusion of the data after the processing of the PET.

5.5 PET processing

Within this Section will be presented the details of the processing steps applied to the PET images, in order to select the most metabolic active spots. These parts are the one of interest because they can be organs, such as the heart or tumor; in fact, as explained in Section 2.2, such areas are masses highly active since they require a considerable amount of blood.

The first step is to rescale the PET images to the dimension of the CT to have comparable results that can be later on merged. Keeping in mind what has been said in Section 5.2, the dimensions of the PET can vary between the helical acquisition and the standard one. In both cases, the resizing of the PET is performed with the nearest-neighbor interpolation method,

where the value of the output pixel is assigned considering only the value of the pixel the point falls within. Thanks to this technique, the information contained in the original image are not altered by the rescaling process. Considering now the helical acquisition, the rescaling has been done by reading in the PET meta-data x or y dimension and the corresponding one on the CT. By dividing the latter for the former it is possible to obtain the ratio needed for the rescale of the PET. On the other hand, this approach cannot be used for the standard acquisition because the PET contains a wider border with respect to the CT.

Giving the PET information about the activity of a certain area, it is possible to identify different levels of activation. This identification is based on a threshold that, for the considered case, has been chosen experimentally in relation to the maximum value present in the image. In this way, it is possible to keep only the highly active regions that correspond to the tumors and disregarding the less informative parts. After this step, the image is composed of a certain number of separated blobs, which correspond to the active spots in the body, so they can be employed for the location of these parts in the merging process.

Having defined the connected blobs that are above the threshold, it is now possible to label them in order to count them and obtain information about their dimension. This process is done by giving a label starting from 1 to N , where N is the number of blobs present in the image. In this way the output image background is set to zero and the pixels belonging to the n th blob have all the value of n . Also this procedure is based on the connected components algorithm and, in this case, the chosen connectivity is 8, as shown in Figure 6.

Having labeled the blobs in the image, it is now possible to obtain information about their geometric properties such as the area and the position of the centroid for each of them. Both of these parameters will be used in the merging process: in fact, the position of the centroid will be used for identifying on the CT the position of the tumor and the border of that specific structure. Moreover, the value of the blob area will be used as parameter for a further step in the fusion of the data: in fact, this value will be employed in the active contouring phase.

5.6 CT and PET fusion

This Section introduces the implemented steps to finally identify the tumor contour on the CT and, being the CT intrinsically more spatially accurate if compared to the PET, to obtain a more accurate identification. As explained in Section 5.5, the position of the blob centroids have been identified, so now it is possible to map those coordinates on the corresponding CT.

Considering that on the PET there was no restrictions for the position of the blobs, some centroid can be on structures such as the heart or other organs that are not useful, since they are out of the scope of this project. For this reason, it is necessary to remove the centroids that are positioned outside the lungs. This procedure can be done by verifying that the value of the pixel correspondent to each identified centroid differs from black within the CT. To do so, there is the need to round the position value of the centroids, because being a geometric characteristic, it can differ from an integer, while the pixels can have only integer indexes of coordinates.

For the aforementioned reasons, if the value of the centroid on the CT is equal to 0 it means that the correspondent blob on the PET is not significant and should be deleted. To remove a

selected blob from the PET mask it can be used its label. In fact, as previously explained, the labeling of the image assigns to all the pixels belonging to a certain blob the same value. Such value can be changed to 0 to cancel the blob from the mask.

To explain the final step that will lead to the identification of the cancer contour, can be useful to resume what have been done so far and which are the input employed for this procedure. The algorithm employed will use as input:

1. the segmented CT in which are visible only the lungs;
2. the details inside them;
3. the mask obtained from the processing of the PET where the non informative blobs have been removed.

These images are used for an iterative computation that, using the centroid position as a seed on the segmented CT, expands at each iteration the dimension of the selected area until it reaches the border of the structure on the CT. This active contouring procedure is based on the Chan-Vese algorithm, which is based on curve evolution techniques that allows the detection of objects boundaries even if they are not defined by gradient [66].

This approach stops when it reaches the convergence, which can be reached through a maximum number of iterations or by another parameter that can be chosen between the contraction bias or the expansion bias (both of them are not dependent on the gradient of the image). In the implemented pipeline the chosen parameter for limiting the expansion is the contraction bias value, which is chosen in relation to the area dimension of the employed blob on the PET. The

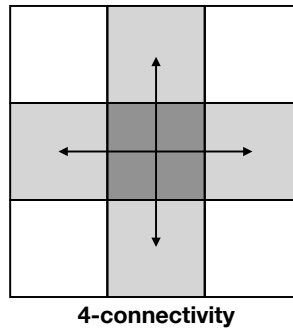


Figure 7: 4-connectivity representation

output image is a binary image where the only white details are the shape of the tumors, which will be later mapped as a contour on the initial CT allowing both a clear visualization of the results from the physician and a further computation for a possible feature extraction, allowing the creation of the standard dataset that can be useful in a machine learning classification of the tumors.

To conclude the pipeline, it is necessary to obtain the contour of the tumor in order to highlight it on the input CT. The border of the previously obtained blob is done by a function that identifies the perimeter of an object in a binary image. The contour is so defined as a pixel that divides a light region from a dark one. In particular, a pixel belonging to the perimeter should be non-zero and it should be connected to at least a zero-valued pixel. The chosen connectivity considered for the decision making process is 4, as proposed in [63], so only the pixel in the main orthogonal directions are taken into account as shown in Figure 7.

Having identified the contour, it can be superimposed to the CT resulting in a white border around the selected tumor. It is important to underline that the image will exploit the details given by the good spatial resolution of the CT and provide to the physician a well known and understandable representation of the information obtained by the pipeline.

CHAPTER 6

IMPLEMENTATION

Within this Chapter the implementation details of the image processing pipeline are proposed. Following the structure of Chapter 5, a more precise description of the input and output datatypes is given and the value of some relevant parameters are validated. For the aforementioned reasons the outline of the Chapter will trace the one of Chapter 5 starting in Section 6.1 with a description of the technical details of the dataset. Section 6.2 shows the dataset structure; then, Section 6.3 and Section 6.4 present the preprocessing and the processing steps of the CT, highlighting the important peculiarities. Finally, Section 6.5 and Section 6.6 respectively, deepen the description of the PET processing and the conclusive steps of the pipeline.

6.1 Technical details

The current Section gives all the technical details regarding the employed dataset in addition to the information related to the machinery employed for the images acquisition.

Both the CT and the PET images are in the DICOM[®] file format (*Digital Imaging and Communications in Medicine*), respecting the standard employed in all the medical field applications.

As explained in Section 5.2, the number of acquired images for each patient is not a fixed parameter but depends on the patient height and the physician. Also the thickness of the slices can vary, with respect to the acquisition modality (standard or helical). The standard produces

TABLE I: RELEVANT DETAILS ABOUT THE DATASET ANALYZED

Features	Standard		Helical	
	CT	PET	CT	PET
Slice thickness [mm]	4	2	3.75	3.75
Matrix dimensions in pixels	512x512	128x128	512x512	256x256
Overlap %	0	0	~ 13	~ 13

PET images have a thickness half of the one of the CT; in fact the PET thickness is 2 mm , while the CT has a thickness of 4 mm . The helical has identical thickness for both the PET and the CT (3.75 mm). Moreover it is important to notice another difference between the two acquisition modalities: the standard one acquires a slice before moving to the adjacent region avoiding any overlap, while the helical one presents some overlap between two subsequent slices (the overlap is 0.48 mm , nearly the 13% of the image thickness).

The image size varies from CT and PET and also from the standard to the helical acquisition type: CTs are grayscale 512x512 pixels regardless the acquisition method, while the PET are grayscale 256x256 pixels on helical acquisitions or 128x128 pixels on the standard one. A summary of the underlined differences is reported in Table I.

Going more in detail about what as been said in Section 5.2, the decision of the acquisition method is strictly correlated with the type and the model of the employed machinery; for this study has been employed a *GE Medical System Discovery 690* [67] and a *Siemens Biograph 6* [68]. The former is the one employed for the helical acquisition, while the latter is used for the standard one.

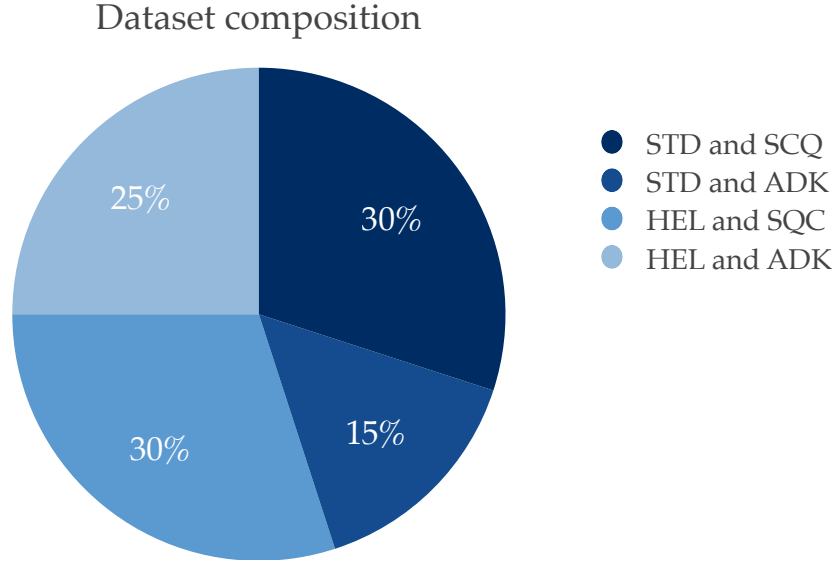


Figure 8: Dataset composition divided by acquisition method and cancer type, where STD=*standard acquisition*, HEL=*helical acquisition*, SQC= *squamous lung cancer* and ADK=*adenocarcinoma lung cancer*

6.2 Dataset structure

For a better understanding of the implemented methodology some considerations should be done on the dataset and on the datatype of the employed images. Both CT and PET are DICOM[®], which is a standard format for medical images and their related information, which allows the storage and the exchange of the data with the required quality for clinical purposes [59]. Moreover, it is recognized as ISO 12052 (International Organization for Standardization) [69] and it is implemented in the majority of the medical imaging devices. For this reason the creation of a pipeline able to manage this file structure is essential for the creation of a diagnostic tool exploitable in the medical field.

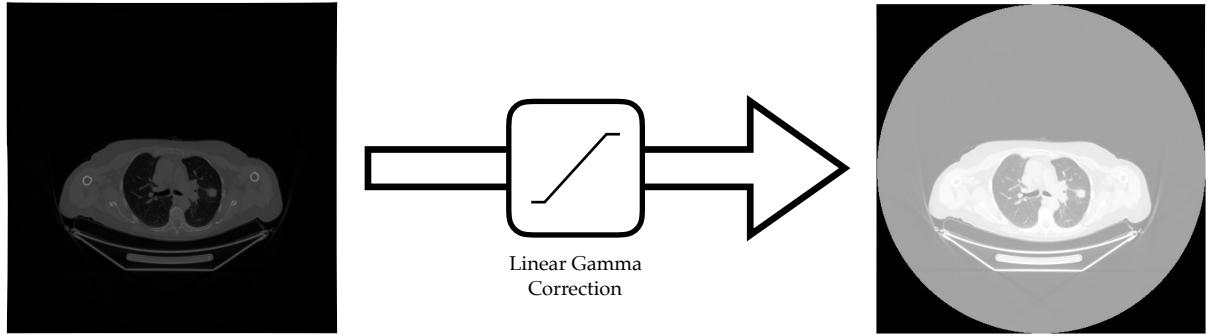


Figure 9: Contrast adjustment with linear gamma correction

The dataset is composed by twenty patients divided, as shown in Figure 8, by acquisition method (standard and helical) and by lung cancer type (squamous and adenocarcinoma). The employed images are composed by the raw image, which is a matrix that, considering both the CT and the PET, is stored as grayscale images with a bit depth of 16 for each pixel. Additionally, the DICOM[®] provides the meta-data structure in which some information are stored such as the dimensions of the matrix containing the acquired image, the image type and the position of each slice based on the integral reference system to the table of the machinery. Considering all these data, each DICOM[®] image is around 520 KB for the CT and 40 KB for the PET, reflecting the different dimensions of the matrices, as reported in Section 6.1.

Meta-data are not reliable information since they can be customized by the different manufacturer. For this reason the created pipeline will rely, when possible, on the image itself instead of such meta-data. Being the aim of this work not only to help the physician in the identification of the cancer lesions but also the creation of a tool able to standardize the creation

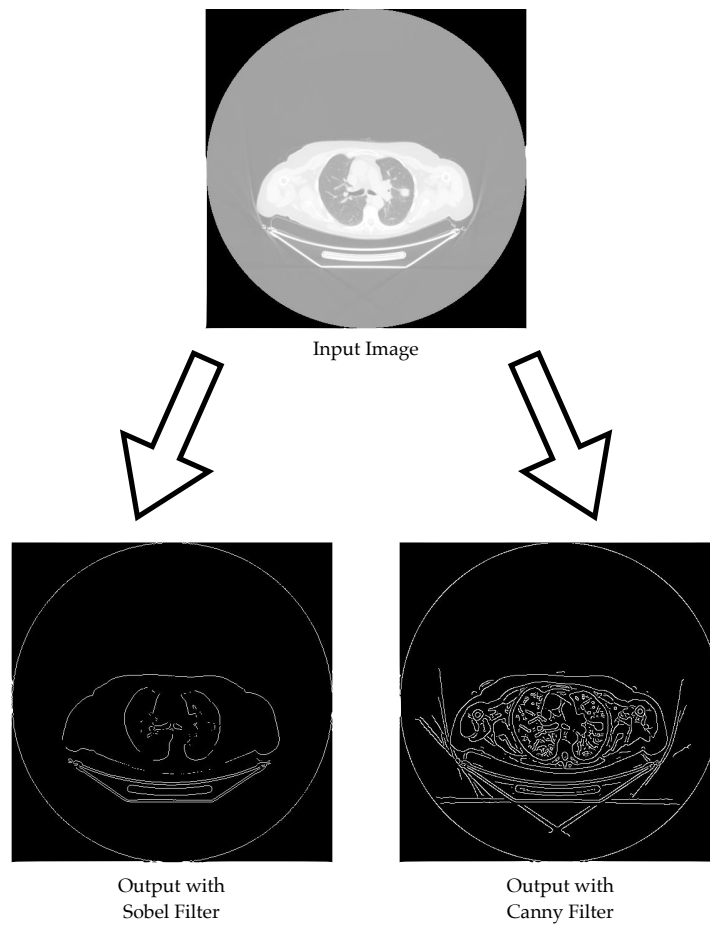


Figure 10: Sobel vs Canny edge detection approaches

of datasets for machine learning approaches, it is clear the need to limit as much as possible the employment of variable characteristics.

6.3 CT preprocessing

Throughout this Section the preprocessing steps applied to the CT images in order to remove the gantry artifact, are explained, with a special focus on the parameters chosen.

As already introduced in Section 5.3 not all the CT images present the gantry artifact which has been defined as the circular shadow around the patient that prevents the correct working of the processing pipeline. In order to identify its presence and the subsequent elimination, as first step an adjustment of the contrast has been performed using a gamma correction algorithm. As visible in Figure 9, starting from a grayscale image the output is still a grayscale image where the top and bottom 1% of all the pixel values are saturated.

On the obtained adjusted image it is now possible to apply the edge detection using the Sobel kernel which, if compared to the Canny [70] one, is able to identify in a more precise way the contour of the patient's torso and the gantry border. As shown in Figure 10, the Canny based approach detects more details if compared to Sobel, but for the purpose of the subsequent step, so many contours limit the wanted result. In fact, the result of the edge detection algorithm will be subtracted to the output of the binarization done with Otsu's method to create the mask employed for the removal of the gantry artifact, as reported in Figure 11.

6.4 CT analysis

In this Section all the relevant details regarding the lungs segmentation are reported, starting from the binarization of the previously preprocessed CT until the final selection of the Region of Interest (ROI).

As already explained in Section 5.4, the binarization has been performed exploiting the iterative Otsu's procedure for the selection of the optimal threshold. On the binarized image, a selection of the biggest connected component has been done using a connectivity equal to 8

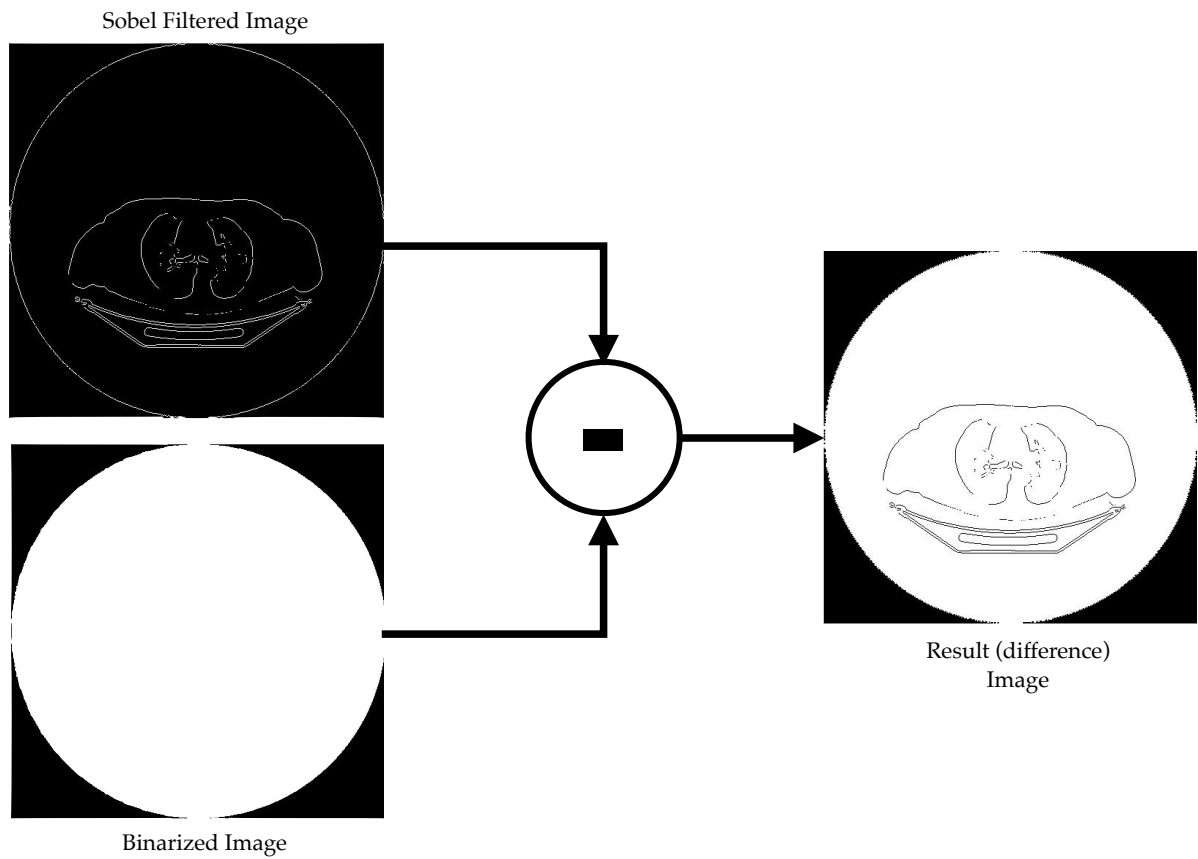


Figure 11: Creation of the mask that will be employed for the removal of the gantry artifact

(see Figure 6) obtaining the body of the patient and some of the internal details of the lungs, as visible in Figure 12.

For the creation of the mask that will be later used for segmenting the lungs it is necessary to obtain a binary image where only the lungs should appear as white spots; moreover, all the small details inside of them, still visible in Figure 12, should be deleted. In order to obtain

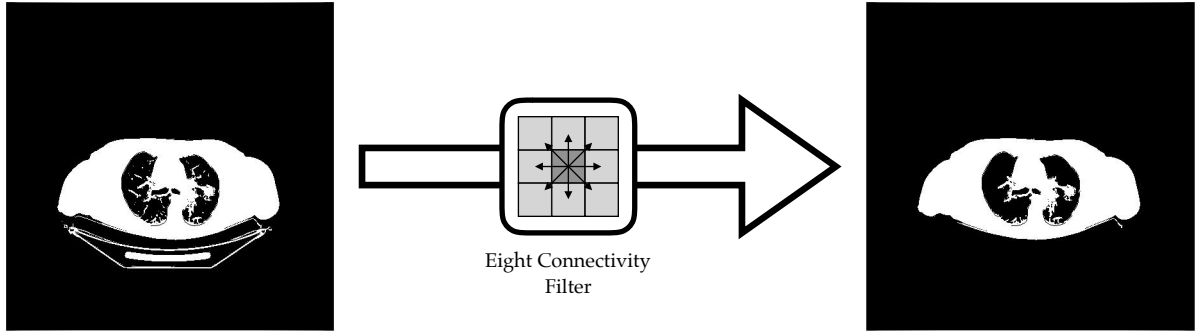


Figure 12: Identification of the largest connected component based on the 8-connectivity filter

the aforementioned mask there is the need to generate the complementary and to modify the background in order to keep it black (Figure 13).

As said in Section 5.4, this approach is based on the suppression of structures that are connected to the image border and that result lighter if compared to their eight adjacent pixels. So considering that all the pixels outside the thorax are white they certainly are lighter compared to it. Moreover, they are all connected to the image perimeter according to the definition of 8-connectivity. Satisfying both the conditions all the pixels outside the thorax can be set to black (background).

Having correctly selected the contour of the lungs, there is now the need of creating a mask, where all the small linear structures inside the lungs are removed in order to make them identifiable later on during the merging of the data coming from both the PET and the CT. In fact, all the details inside the lungs should be preserved on the original CT after the filtering with the created mask, since they can be possible tumors. The applied technique for the removal

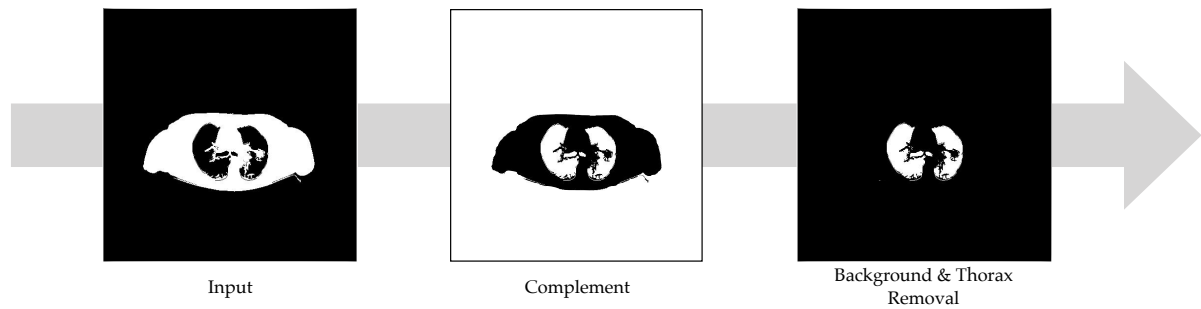


Figure 13: From the input to the background and thorax removal within the lungs identification process

of the linear structures is a morphological closure of the image, which, as explained in Section 5.4, is a procedure composed of two sequential steps: a dilation followed by an erosion. These algorithms require the employment of a constructing element, which is used to probe the pixels surrounding the one selected and to decide if that specific element is part of a structure similar to the shape of the probe. The dilation process fills the possible holes present in the image in order to better fit the shape of the constructing element, while the erosion has the opposite effect.

Applying the dilation followed by the erosion allows the preservation of those shapes that match the chosen probe and the filling of possible white isolated pixels inside those regions. Taking into account what have been said, in order to remove the linear ramification departing from the central structure, it has employed a round structuring element for preserving only the circular shaped region. At this point it is necessary to chose the radius of the probing circular element.

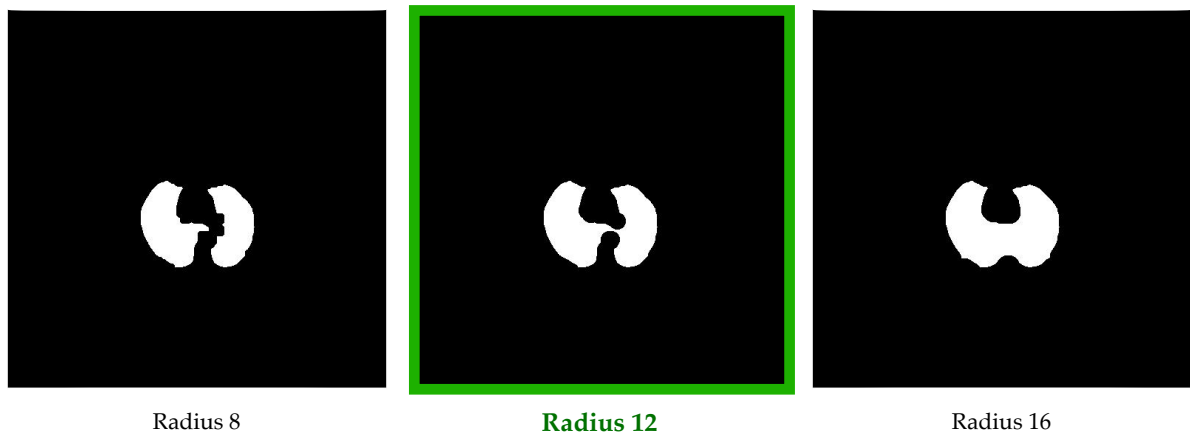


Figure 14: Morphological closure with different constructing element radius; the green one is the selected one

Figure 14 shows some attempts with different radii: experimentally it has been found that a good trade off is a radius equal to 12, which is the one not only able to remove all the linear structures but also to preserve the main circular shaped regions.

Now that the mask has been obtained, the last step of the CT processing pipeline is the filtering of the preprocessed image with the morphological closed image. In this way the segmented ROI corresponding to the lungs contour and their inside details is obtained (Figure 15).

6.5 PET analysis

Having reached the aim of the CT processing it is now useful to introduce more details about what has been performed in order to extract the necessary information from the PET acquisition. Throughout the Section a deeper explanation of some implemented algorithms will be given.

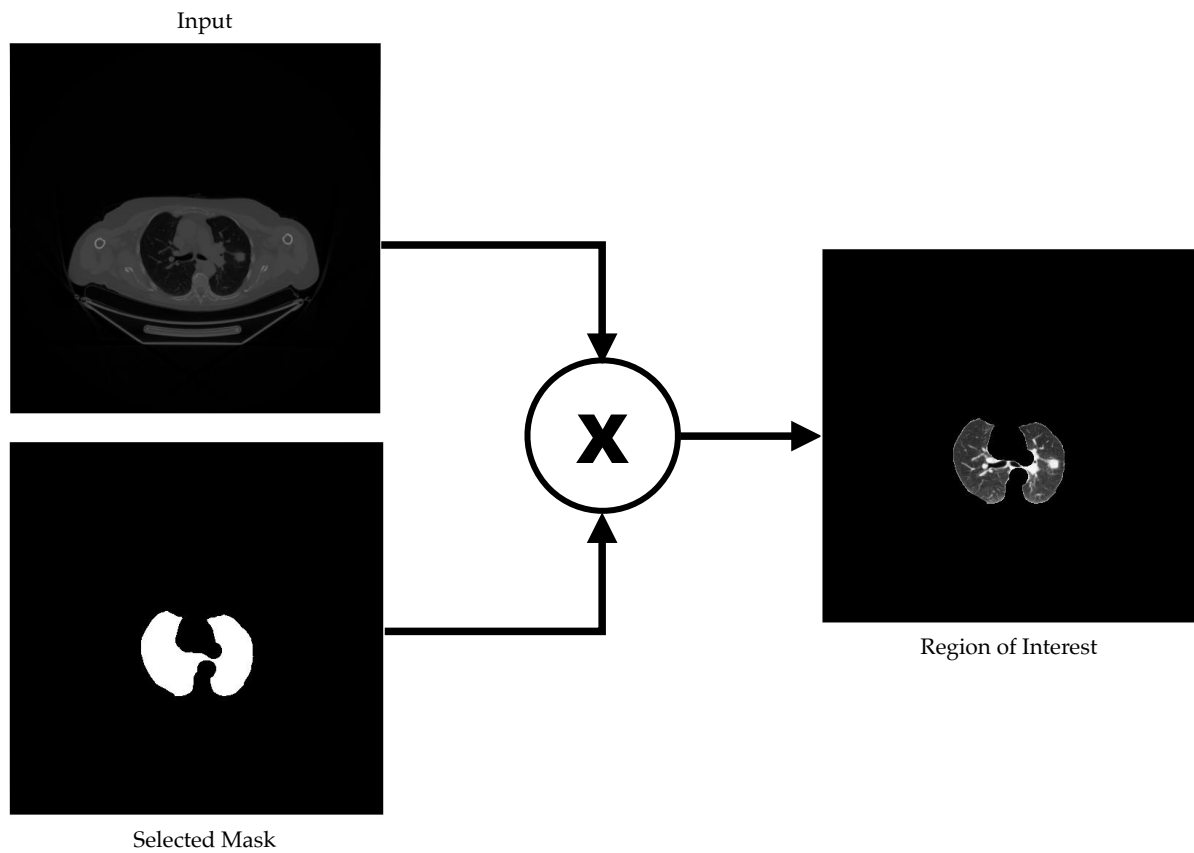


Figure 15: Identification of the Region of Interest within the CT processing pipeline

As said CT and PET have different image sizes, so a rescaling step is required for the next steps of the processing pipeline (1:1 mapping needed). In order to do not lose information by reducing the CT to the smaller dimensions of the PET and to provide results that can be more easily seen on a larger image, it is better to upscale the PET to the CT dimensions. For the aforementioned reasons, it has been used the metadata for reading the dimension values of the

CT and then employ them as parameters for the scaling of the PET using the nearest neighbor algorithm.

Having now comparable images in terms of dimension, it is possible to begin with the real processing steps. The first one consists in thresholding the PET based on the maximum value in it. Experimental studies showed that good results can be achieved by using as decision value the 80% of the maximum. Using a higher or lower threshold leads to respectively an under or over identification of the active spots, falsifying the final result.

Obtained the informative regions, it is necessary to label each blob in order to compute the position of the centroid and the area. The procedure gives to the pixel belonging to a certain blob the same value on the base of the 8-connectivity definition. The final result of the PET analysis is therefore a mask where, for each active spots, are computed the area and the position (x_c, y_c) of the centroid, as reported in Equation 6.1. In such Equation, N is the total number of pixels composing the blob; x_i and y_i are the x, y positions of the N pixels respectively. Finally, the area value is the algebraic sum of the pixels belong to the blob.

$$x_c = \frac{1}{N} \sum_{i=1}^N x_i, \quad y_c = \frac{1}{N} \sum_{i=1}^N y_i \quad (6.1)$$

6.6 Cancer lesion identification

Considering now the concluding part of the pipeline, more details will be presented for clarifying how the contour identification is performed and which information are exploited from both sources.

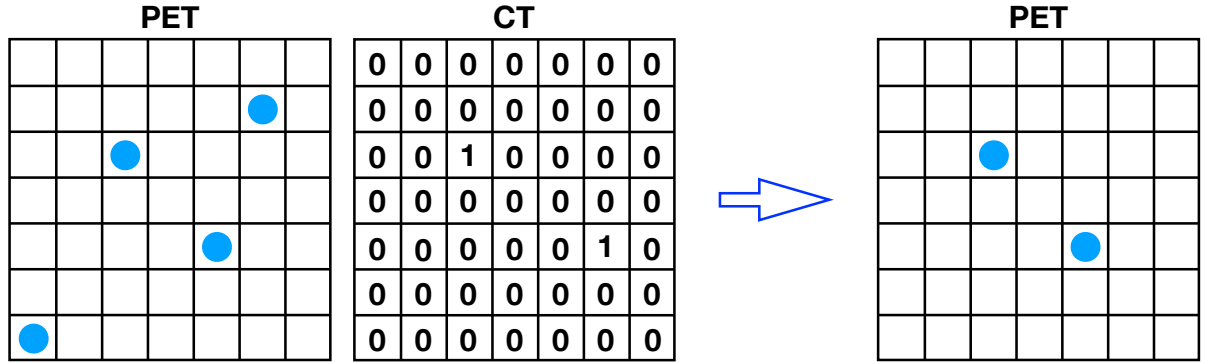


Figure 16: Removal of PET centroid based on the CT corresponding values

First of all, the segmented CT is used as delimitation to distinguish between interesting centroids that are inside the lungs region and centroids that are positioned in non informative areas, such as the heart or the ribcage. In fact, the centroid identification on the PET is done on the base of the intensity and not on the base of the position inside the patient's body: consequently a merge of the information is essential.

For eliminating the centroid that are obtained from blobs that are located outside the Region of Interest, as said in Section 5.6, a check has been done on the value of the CT pixel corresponding to the centroid position on the PET (Figure 16): if the CT value is equal to zero, that centroid is positioned in a region that is not part of the Region of Interest and, for this reason, it will be eliminated from the PET mask. On the other hand, if the pixel value on the CT differs from zero, it means that the centroid is inside the lungs and will be then considered for the identification of the contour of the tumor. The implemented steps used for this procedure are reported in Algorithm 3

Data: input labeled PET image
Data: input segmented CT image
Result: Blob centroids inside ROI
stats[n_blob] \leftarrow position of blob centroids in input image;
blob[n_blob] \leftarrow labeled blob in the input image;
for $i=1, \dots, n_blob$ **do**
 if $CT(stats[n_blob])=0$ **then**
 blob[n_blob]=0;
 end
end

Algorithm 3: Pseudocode for removing the blobs outside the ROI on labeled PET image

Having stored only the position of the useful blobs, it is now possible to employ them as seed for the identification of the contour of the tumor on the CT as seen in Figure 17.

The algorithm employed for the definition of the contour is an iterative procedure that, starting from a pixel (identified centroid) at each iteration, expands the seed of a certain number of pixels, until the contour of the structure containing the starting pixel is reached. In order to limit the expansion of the area over the real border of the tumor, there is the necessity to have a termination condition of the iterative algorithm. This can be done considering a maximum number of iterations or using a parameter that, if positive, bias the contour to shrink inwards, limiting in this way the excessive expansion. Considering the specific case, the limitation method that has been applied is the one based on the contraction bias; the contraction parameter has been set to a value obtained in Equation 6.2

$$contraction = \frac{Area}{100} - 0.18 \quad (6.2)$$

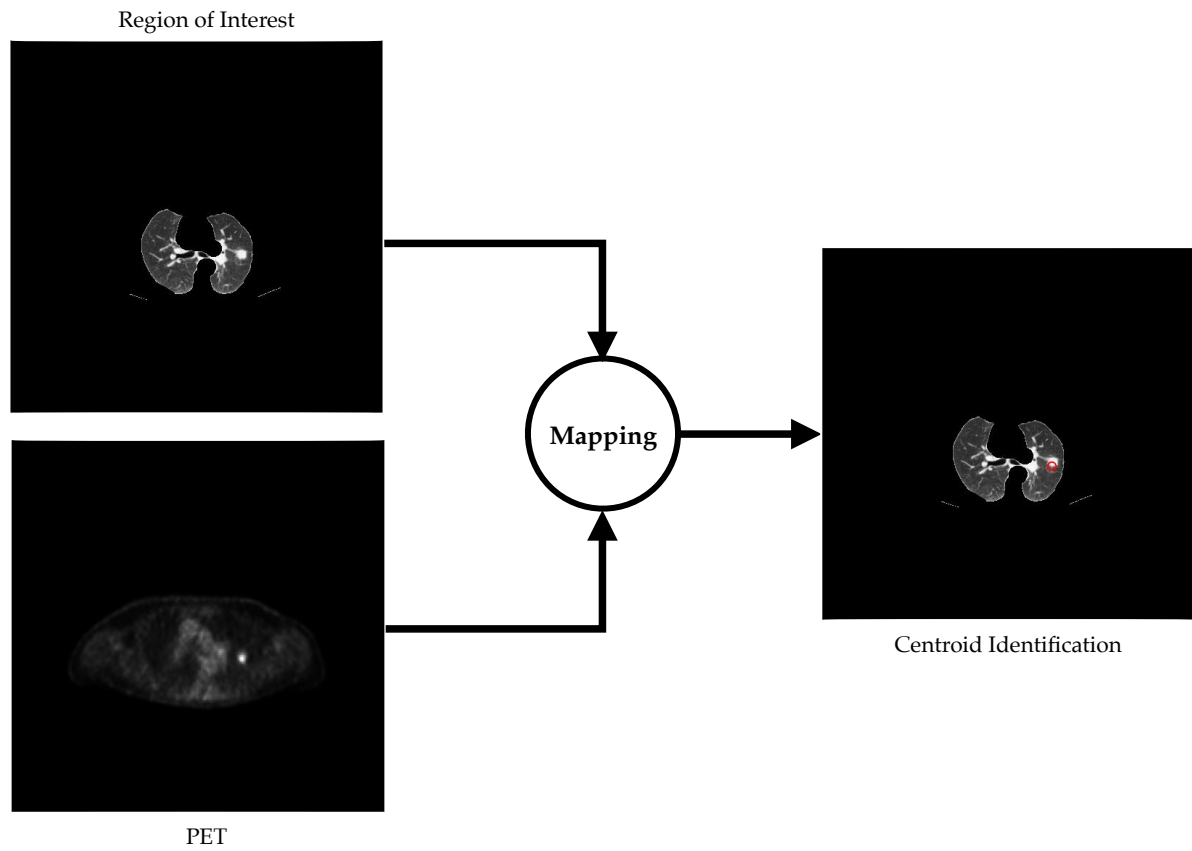


Figure 17: Identification of the valid centroid inside the Region of Interest

The algorithm used for the active contour approach is the Chan-Vese: this algorithm does not employ edges for the identification of the perimeter of the image, but exploits information about energy, being capable of identifying objects whose contours are not defined by the gradient [66]. This approach relies on the minimization of a energy function, which reaches its minimum value when it matches the contour of the object, while, if the curve is inside or outside the object, it will be respectively lesser or greater of zero. For this reason, this approach is able to

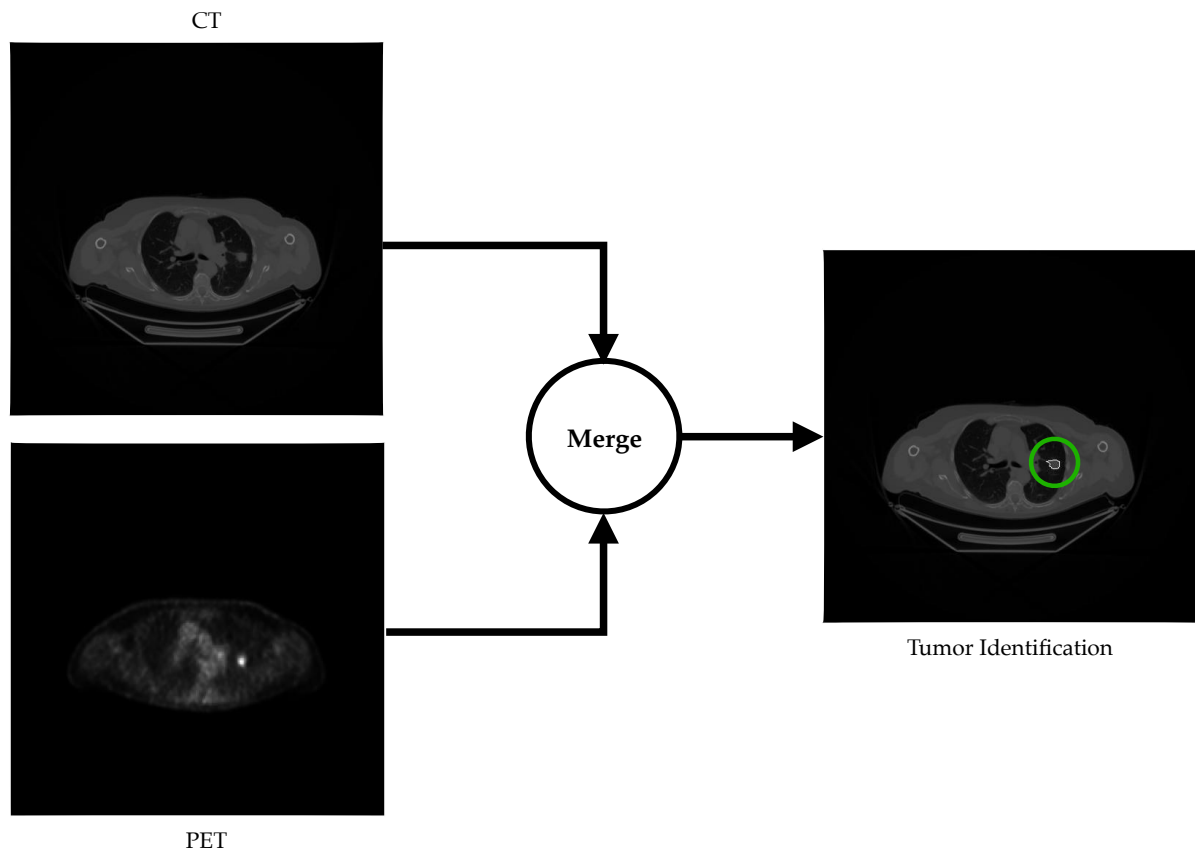


Figure 18: Final identification of the contour of the lungs cancer lesion

detect not only objects with clear boundaries, but also structure with smooth of discontinuous edges, being suitable for the identification of tumors, even if they are surrounded by tissues with similar properties. In the analyzed case study, the starting position of the contour is given by the perimeter of the blobs that has been identified from the PET. By using that profile as starting point, the minimization of the energy function has been done then on the segmented CT.

The output obtained by the contour algorithm is a binary image where it is possible to see white regions corresponding to the areas on the CT, where a tumor should be found. Starting from these data, it is then possible to keep only the perimeter of those structures (the entire blob), by keeping only those pixels that are part of the structure and are connected to other pixels of the object and separate a dark region from a light one.

Finally, to obtain an easily readable result, the contour of the identified tumors is mapped on the original CT, allowing the physician to detect the presence of a cancer lesion thanks to white contour around it (Figure 18). The reason behind this choice is to do not modify the routine employed in this field for the diagnosis, which consists in the examination of CT or PET images. Moreover, by reporting the contour on the input image the information in it contained is not modified both in terms of dimensions and spatial resolution, obtaining an image already usable by a radiologist.

CHAPTER 7

EXPERIMENTAL EVALUATION

This Chapter presents the approached used for the validation of the pipeline and the obtained results both in term of execution time and accuracy compared to the semi-automatic segmentation method employed by the radiologists. In detail, Section 7.1 describes the experimental setup in terms of language and framework used, and target device; Section 7.2 presents the results obtained in terms of execution time. Finally, Section 7.3 provides the information about the accuracy obtained by the implemented pipeline.

First of all, remembering what was said in Section 3.3, it is impossible to directly compare the obtained results with the ones in literature due to the lack of reproducibility of the works; for this reason, within this work, the validation will be done considering the information provided by the physicians who have collected the data.

7.1 Experimental setup

The developed pipeline has been implemented in MATLAB_R2017b[®] (a MathWorks[®] product), which is a language created for technical computing [71] and an environment that allows the data analysis, algorithm development and data visualization. MATLAB[®] has been chosen as development tool since it is employed in multiple field such as biotechnology, finance, industry and research. All the computation has been performed on a MacBook Pro with a 3.1 GHz Intel Core i5 with a 16 GB 2133MHz LPDDR3 RAM memory.

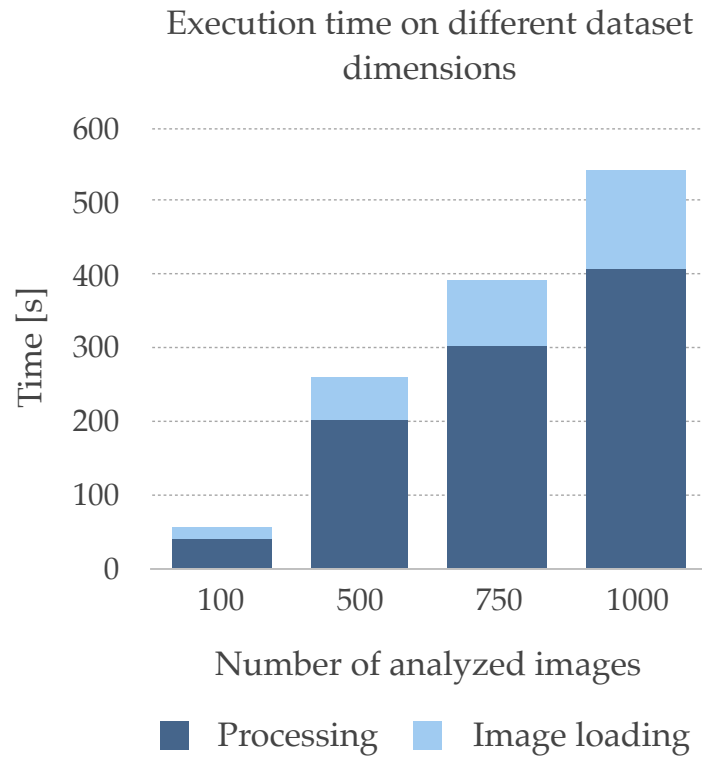


Figure 19: Execution time on different dataset dimensions

7.2 Execution time

Considering the execution time, an expert radiologist usually employs between five and ten minutes to analyze a patient acquisition; this time may further increase if the physician is distracted by external factors or if he/she is working from too many hours. Looking at Figure 19 and keeping in mind that generally a single acquisition is composed by 200-300 images, the proposed tool is able to analyze the same number of images in less than three minutes. Figure 19 reports the execution time measured on different dataset dimension (from

100 images to 1000 images). The experimental results show that the computation time goes from 52.89 seconds for 100 images to 540.65 second for 1000 images. Figure 19 does not shows the standard deviation since it is not significant: however it ranges between 0.02 and 0.04. Moreover, as it is possible to notice from the same Figure, considering only the pure computation time without the image loading from the disk, execution time is reduced by 20%.

In addition, increasing the number of images, the execution time grows pretty much linearly, while, on the contrary, a physician will decrease the performance in terms of analysis time with the increase of the number of images analyzed due to his/her tiredness. It is important to notice that it is possible also to further reduce the total execution time of the proposed tool since it is possible to make some optimizations: as an example, thanks to a statistical analysis, it is possible to discharge a percentage of the acquired slices, which are the ones covering the abdominal region, which is out of the Region of Interest.

7.3 Accuracy

Moving on to the assessment of the accuracy some quantitative statistics have been computed and are listed below:

- True Positive (TP) or number of images containing a lesion correctly identified;
- True Negative (TN) or number of images not containing a lesion correctly identified;
- False Positive (FP) or number of images not containing a lesion incorrectly identified;
- False Negative (FN) or number of images containing a lesion incorrectly identified.

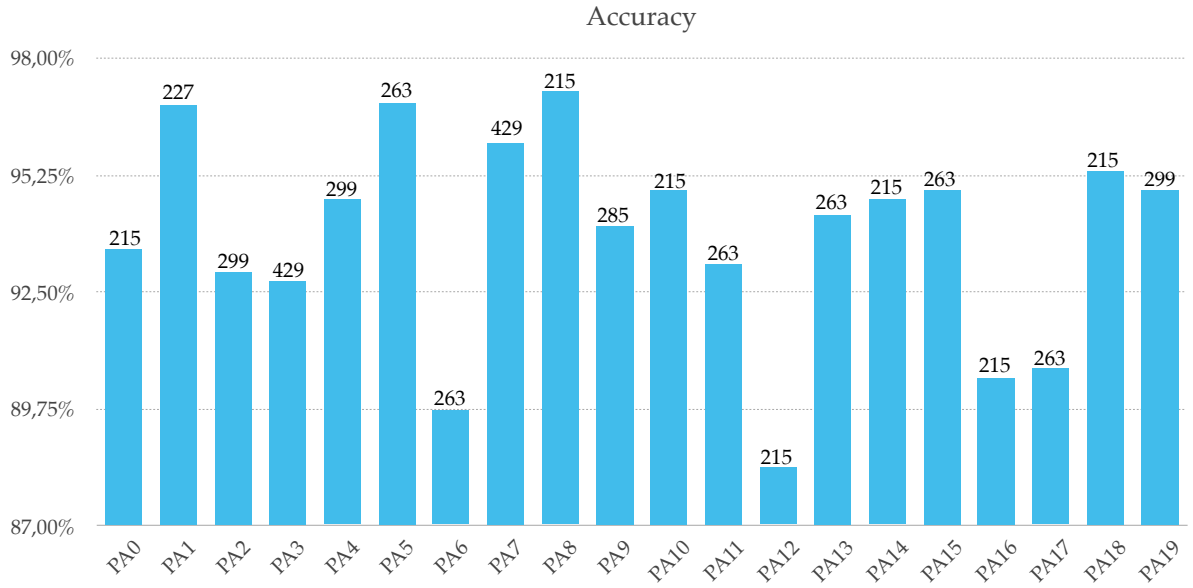


Figure 20: Accuracy obtained for each patient considering the number of analyzed images (the number of images is reported above each bar)

From these parameters it is possible to compute the sensitivity SE (Equation 7.1), the specificity SP (Equation 7.2), and the accuracy ACC (Equation 7.3) with the following formulas.

$$SE = \frac{TP}{TP + FN} \quad (7.1)$$

$$SP = \frac{TN}{TN + FP} \quad (7.2)$$

$$ACC = \frac{TP + TN}{TP + FN + TN + FP} \quad (7.3)$$

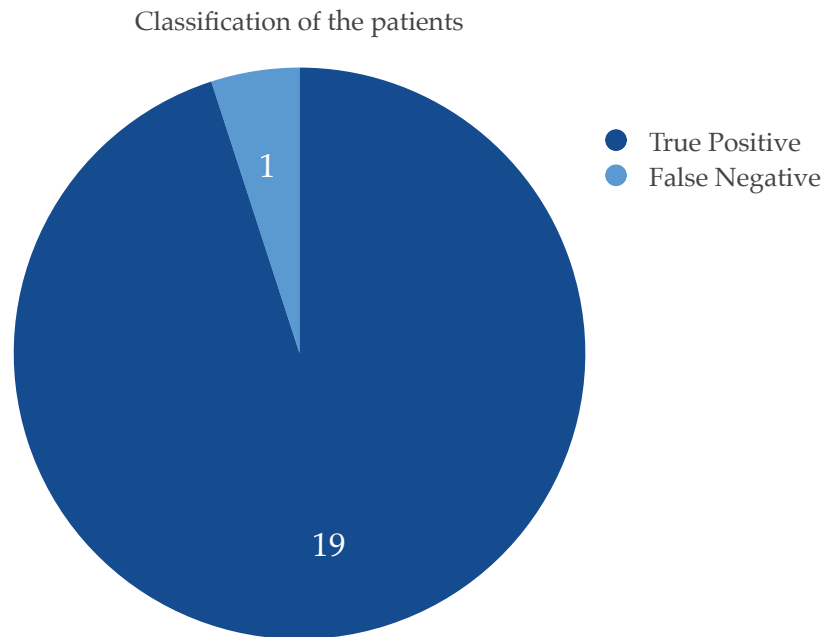


Figure 21: Number of correctly classified vs misclassified patients

For each patient these statistics have been computed using as ground truth the classification done by the radiologist. Figure 20 shows the obtained accuracy for each analyzed patient; it is possible to see that the accuracy varies between 88-97% with a mean value of 93.82%. Moreover, for each patient it is reported the total number of slices acquired during the examination, which varies from a minimum of 215 and a maximum of 429. As reported in Equation Equation 7.3, the accuracy depends on all the correctly identified slices both the TN and the TP; for this reason, in some cases some slices which do not contain the lungs are misclassified as containing a tumor (false positives); in order to increase the accuracy, it can be useful to remove a percentage of images (abdominal and legs areas) decreasing the possibility to create false positive in areas

that are certainly not lungs. This kind of optimization is left as future work. Moreover even if a patient is correctly identified as affected by lung cancer, the first and the last slices containing the tumor are difficult to segment due to the low activity in this terminal part of the tumor.

In addition, considering the obtained results, only one patient with tumor has been misclassified as a sane patient (false negative) (Figure 21). This is generally a bad result, so it is important to investigate the causes of this classification error for future improvements of the methodology. In this case, in fact, even if an abnormal structure is visible on the CT, the ROI identified by the radiologist on the PET is poorly active, leading the algorithm to discharge that part of the image as not informative. This problem, is the same one found in the terminal area of the tumors in the other patients. For this reason later on some studies can be done to overcome this issue. A possible solution left as future work is use information among consecutive slices instead of reasoning on one slice at a time: the idea here is to exploit a 3D connected components algorithm [72].

CHAPTER 8

CONCLUSIONS AND FUTURE WORKS

This thesis work is about the early and accurate diagnosis of lung cancer, one of the most investigated open challenges in the last decades. High attention has been given to the creation of tools that can help physicians in this sense and this project works toward this direction.

Since lung cancer is the second leading death cause between both male and female after prostate and breast cancers [1] it is usually lethal if not detected in early stages, it is crucial an early identification for increasing the possibility of survival of patients with cancer. Therefore this thesis has proposed an automatic diagnostic tool that requires less time for the identification (compared to a physician) and does not require a cross-validation of the results by different radiologists, being in this way cheaper and less error prone.

A deep analysis of the related works has been performed: starting from the current imaging technologies, such as *Computed Tomography* (CT) and *Positron Emission Tomography* (PET), very different solutions have been proposed in literature for an accurate and fast identification of lung cancer. However, the found solutions are generally based on semi-automated protocol where the radiologist manually draws the Region Of Interest (ROI) and, after that, a program inside the decided ROI segments the tumor masses. This approach can be useful but it is not enough. In fact, in the last years, some new fully automated identification tools have been proposed but they do not show how their algorithms have been implemented in details.

Given the aforementioned context, this work output tries to make a step forwarding into the field having proposed a completely automated pipeline able to be a reference standard able to identify lung cancer, that can be employed for the clinical follow up and that can be a suitable starting point for a machine learning based classification procedure.

Being more precise, this thesis proposed both a methodology and the related software tool that taking as input *Digital Imaging and COmmunications in Medicine* (DICOM) files of chest PET and CT and, by exploiting the characteristics of both of them, is capable of automatically identifying the lungs and the possible presence of tumor lesions.

A validation of the pipeline has been done by computing the execution time and the accuracy of the processing pipeline. With respect to the execution time, the computation time goes from 52.89 seconds for 100 images to 540.65 seconds for 1.000 images. This is a considerable result since an expert radiologist usually employs between five and ten minutes to analyze a patient acquisition. With respect to the accuracy it varies between 89-97% on the analyzed dataset.

Future Works

The experimental results shown as the obtained accuracy varies between 88-97%. In some cases some slices which do not contain the lungs have been misclassified as containing a tumor (false positives); in order to increase the accuracy, as future work it is possible to automatically remove a percentage of images (abdominal and legs areas) decreasing the possibility to create false positive in areas that are certainly not lungs. Moreover, in one case, an affected patient has been classified as healthy (false negative): analysis on that patient showed that the ROI identified by the radiologist on the PET was poorly active, leading the algorithm to discharge

that part of the image as not informative. To solve this kind of issues it is possible to use information among consecutive slices instead of reasoning on one slice at a time. This is possible for instance by using 3D connected components algorithm able to reconstruct a volume among consecutive 2D projections.

As said, a further step for the reduction of the mortality rate due to lung cancer can be seen in machine learning approaches which, exploiting the information obtained from the many segmentation, are able to provide information regarding the tumor. Therefore, a possible next step for this project is to implement new classification algorithms based on machine learning which exploit the data generated from the proposed pipeline. However, such kind of methodologies require huge dataset as inputs. This means that accelerating the proposed algorithms on more powerful hardware can be a necessary step to make the creation of the dataset feasible: working on GPUs platforms can be a good match, since they are designed to perform graphical analysis.

APPENDICES

Appendix A

COPYRIGHT PERMISSION 1

This appendix include the terms under which is copyrighted Figure 1.

Images available through this page and commons.wikimedia.org/wiki/File:Lungsdiagram_simple.svg are made available under Creative Commons CC BY 2.5 License 2006. Creative Commons Attribution 2.5 License 2006 allows you to:

To Share: Copy, Distribute, and Transmit the work,

To Remix: To adapt the work.

To Remix: Create Derivative works of the material under these conditions: **Attribution:** You must attribute the work in the manner specified by the author or licensor (but not in any way that suggests that they endorse you or your use of the work).

Appendix B

COPYRIGHTS PERMISSION 2

This appendix include the terms under which is copyrighted Figure 2.

Images available through this page and https://commons.wikimedia.org/wiki/File:Diagram_showing_how_cancer_cells_keep_on_reproducing_to_form_a_tumour_CRUK_127.svg are made available under Creative Commons CC BY-SA 4.0 International license.. Creative Commons Attribution-Share Alike 4.0 International license allows you to:

To Share: Copy, Distribute, and Transmit the work,

To Remix: To adapt the work.

To Remix: Create Derivative works of the material under these conditions: **Attribution:** You must attribute the work in the manner specified by the author or licensor (but not in any way that suggests that they endorse you or your use of the work). This image has been released as part of an open knowledge project by Cancer Research UK. **Share alike:** If you alter, transform, or build upon this work, you may distribute the resulting work only under the same or similar license to this one.

CITED LITERATURE

1. Hossain, M. R. I., Ahmed, I., and Kabir, M. H.: Automatic lung tumor detection based on glcm features. In Asian Conference on Computer Vision, pages 109–121. Springer, 2014.
2. Cancer details. <https://www.medicinenet.com/script/main/art.asp?articlekey=2580>. Accessed: 2018-03-20.
3. Survival rate for nslc. <https://www.cancer.org/cancer/non-small-cell-lung-cancer/detection-diagnosis-staging/survival-rates.html>. Accessed: 2018-03-14.
4. Kim, Y. J., Lee, S. H., Lim, K. Y., and Kim, K. G.: Development and validation of segmentation method for lung cancer volumetry on chest ct. Journal of digital imaging, pages 1–8, 2018.
5. Kuruvilla, J. and Gunavathi, K.: Lung cancer classification using neural networks for ct images. Computer methods and programs in biomedicine, 113(1):202–209, 2014.
6. Pawełczyk, K., Kawulok, M., Nalepa, J., Hayball, M. P., McQuaid, S. J., Prakash, V., and Ganeshan, B.: Towards detecting high-uptake lesions from lung ct scans using deep learning. In International Conference on Image Analysis and Processing, pages 310–320. Springer, 2017.
7. Kumar, S. L., Swathy, M., Sathish, S., Sivaraman, J., and Rajasekar, M.: Identification of lung cancer cell using watershed segmentation on ct images. Indian Journal of Science and Technology, 9(1), 2016.
8. Soufi, M., Kamali-Asl, A., Geramifar, P., and Rahmim, A.: A novel framework for automated segmentation and labeling of homogeneous versus heterogeneous lung tumors in [18 f] fdg-pet imaging. Molecular Imaging and Biology, 19(3):456–468, 2017.
9. Cui, H., Wang, X., Lin, W., Zhou, J., Eberl, S., Feng, D., and Fulham, M.: Primary lung tumor segmentation from pet-ct volumes with spatial-topological constraint. International journal of computer assisted radiology and surgery, 11(1):19–29, 2016.

CITED LITERATURE (continued)

10. Parmar, C., Grossmann, P., Bussink, J., Lambin, P., and Aerts, H. J.: Machine learning methods for quantitative radiomic biomarkers. Scientific reports, 5:13087, 2015.
11. Kourou, K., Exarchos, T. P., Exarchos, K. P., Karamouzis, M. V., and Fotiadis, D. I.: Machine learning applications in cancer prognosis and prediction. Computational and structural biotechnology journal, 13:8–17, 2015.
12. Beachey, W.: Respiratory care anatomy and physiology: foundations for clinical practice. Elsevier Health Sciences, 2018.
13. Broaddus, V. C., Mason, R. C., Ernst, J. D., King, T. E., Lazarus, S. C., Murray, J. F., Nadel, J. A., Slutsky, A., and Gotway, M.: Murray & Nadel's Textbook of Respiratory Medicine E-Book. Elsevier Health Sciences, 2015.
14. Hall, J. E.: Guyton and Hall textbook of medical physiology e-Book. Elsevier Health Sciences, 2015.
15. Corrin, B. and Nicholson, A. G.: Pathology of the Lungs E-Book: Expert Consult: Online and Print. Elsevier Health Sciences, 2011.
16. Cancer definition. <https://www.cancer.gov/publications/dictionaries/cancer-terms/def/cancer>. Accessed: 2018-03-14.
17. Kerr, J. F., Wyllie, A. H., and Currie, A. R.: Apoptosis: a basic biological phenomenon with wideranging implications in tissue kinetics. British journal of cancer, 26(4):239, 1972.
18. Elmore, S.: Apoptosis: a review of programmed cell death. Toxicologic pathology, 35(4):495–516, 2007.
19. Cancer description. <https://www.cancer.gov/about-cancer/understanding/what-is-cancer>. Accessed: 2018-03-14.
20. Non small cell lung cancer. <https://www.cancer.org/cancer/non-small-cell-lung-cancer/about/what-is-non-small-cell-lung-cancer.html>. Accessed: 2018-04-03.
21. Kawase, A., Yoshida, J., Ishii, G., Nakao, M., Aokage, K., Hishida, T., Nishimura, M., and Nagai, K.: Differences between squamous cell carcinoma and adenocarcinoma of

CITED LITERATURE (continued)

- the lung: are adenocarcinoma and squamous cell carcinoma prognostically equal? Japanese journal of clinical oncology, 42(3):189–195, 2011.
22. General, S.: The health consequences of smoking?50 years of progress: a report of the surgeon general. In US Department of Health and Human Services. Citeseer, 2014.
 23. Alberg, A. J. and Samet, J. M.: Epidemiology of lung cancer. Chest, 123(1):21S–49S, 2003.
 24. Siegel, R. L., Miller, K. D., and Jemal, A.: Cancer statistics, 2018. CA: a cancer journal for clinicians, 68(1):7–30, 2018.
 25. Biopsy. <https://www.cancer.gov/publications/dictionaries/cancer-terms/def/biopsy>. Accessed: 2018-04-03.
 26. X-rays. <https://www.cancer.gov/publications/dictionaries/cancer-terms/def/x-ray>. Accessed: 2018-03-22.
 27. Computed tomography. <https://www.nibib.nih.gov/science-education/science-topics/computed-tomography-ct>. Accessed: 2018-03-21.
 28. Positron emitting products. <https://www.fda.gov/Radiation-EmittingProducts/RadiationEmittingProductsandProcedures/MedicalImaging/MedicalX-Rays/ucm115317.htm>. Accessed: 2018-03-21.
 29. Miqueles, E., Koshev, N., and Helou, E. S.: A backprojection slice theorem for tomographic reconstruction. IEEE Transactions on Image Processing, 27(2):894–906, 2018.
 30. Ct resolution. <http://www.ctlab.geo.utexas.edu/about-ct/resolution-and-size-limitations/>. Accessed: 2018-03-21.
 31. Liguori, C., Frauenfelder, G., Massaroni, C., Saccomandi, P., Giurazza, F., Pitocco, F., Marano, R., and Schena, E.: Emerging clinical applications of computed tomography. Medical Devices (Auckland, NZ), 8:265, 2015.
 32. Nuclear medicine. <https://www.nibib.nih.gov/science-education/science-topics/nuclear-medicine>. Accessed: 2018-03-21.
 33. Shibuya, K., Yoshida, E., Nishikido, F., Suzuki, T., Tsuda, T., Inadama, N., Yamaya, T., and Murayama, H.: Annihilation photon acollinearity in pet: volunteer and phantom fdg studies. Physics in Medicine & Biology, 52(17):5249, 2007.

CITED LITERATURE (continued)

34. Moses, W. W.: Fundamental limits of spatial resolution in pet. Nuclear Instruments and Methods in Physics Research Section A: Accelerators, Spectrometers, Detectors and Associated Equipment, 648:S236–S240, 2011.
35. Wernick, M. N. and Aarsvold, J. N.: Emission tomography: the fundamentals of PET and SPECT. Elsevier, 2004.
36. Kaira, K., Oriuchi, N., Sunaga, N., Ishizuka, T., Shimizu, K., and Yamamoto, N.: A systemic review of pet and biology in lung cancer. American journal of translational research, 3(4):383, 2011.
37. Szyszko, T. A., Yip, C., Szlosarek, P., Goh, V., and Cook, G. J.: The role of new pet tracers for lung cancer. Lung Cancer, 94:7–14, 2016.
38. Hirsch, F. R., Franklin, W. A., Gazdar, A. F., and Bunn, P. A.: Early detection of lung cancer: clinical perspectives of recent advances in biology and radiology. Clinical Cancer Research, 7(1):5–22, 2001.
39. Tockman, M. S.: Survival and mortality from lung cancer in a screened population: the johns hopkins study. Chest, 89(4):324S–325S, 1986.
40. Miller, A. and Sanderson, D. R.: Lung cancer screening: Screening the mayo study. Chest, 89(4):324S, 1986.
41. Melamed, M. R., Flehinger, B. J., Zaman, M. B., Heelan, R. T., Perchick, W. A., and Martini, N.: Screening for early lung cancer: results of the memorial sloan-kettering study in new york. Chest, 86(1):44–53, 1984.
42. Travis, W. D., Brambilla, E., Nicholson, A. G., Yatabe, Y., Austin, J. H., Beasley, M. B., Chirieac, L. R., Dacic, S., Duhig, E., Flieder, D. B., et al.: The 2015 world health organization classification of lung tumors: impact of genetic, clinical and radiologic advances since the 2004 classification. Journal of thoracic oncology, 10(9):1243–1260, 2015.
43. de Gonzalez, A. B. and Darby, S.: Risk of cancer from diagnostic x-rays: estimates for the uk and 14 other countries. The lancet, 363(9406):345–351, 2004.
44. Chon, A., Balachandar, N., and Lu, P.: Deep convolutional neural networks for lung cancer detection. Technical report, tech. rep., Stanford University, 2017.

CITED LITERATURE (continued)

45. Yan, Z., Zhan, Y., Peng, Z., Liao, S., Shinagawa, Y., Zhang, S., Metaxas, D. N., and Zhou, X. S.: Multi-instance deep learning: Discover discriminative local anatomies for bodypart recognition. IEEE transactions on medical imaging, 35(5):1332–1343, 2016.
46. Hussein, S., Gillies, R., Cao, K., Song, Q., and Bagci, U.: Tumornet: Lung nodule characterization using multi-view convolutional neural network with gaussian process. In Biomedical Imaging (ISBI 2017), 2017 IEEE 14th International Symposium on, pages 1007–1010. IEEE, 2017.
47. Salman, N.: Image segmentation based on watershed and edge detection techniques. Int. Arab J. Inf. Technol., 3(2):104–110, 2006.
48. Levner, I. and Zhang, H.: Classification-driven watershed segmentation. IEEE Transactions on Image Processing, 16(5):1437–1445, 2007.
49. Adams, R. and Bischof, L.: Seeded region growing. IEEE Transactions on pattern analysis and machine intelligence, 16(6):641–647, 1994.
50. Grau, V., Mewes, A., Alcaniz, M., Kikinis, R., and Warfield, S. K.: Improved watershed transform for medical image segmentation using prior information. IEEE transactions on medical imaging, 23(4):447–458, 2004.
51. Ju, W., Xiang, D., Zhang, B., Wang, L., Kopriva, I., and Chen, X.: Random walk and graph cut for co-segmentation of lung tumor on pet-ct images. IEEE Transactions on Image Processing, 24(12):5854–5867, 2015.
52. Undirected graph. https://mathinsight.org/definition/undirected_graph. Accessed: 2018-04-16.
53. Lermé, N., Malgouyres, F., and Létocart, L.: Reducing graphs in graph cut segmentation. In Image Processing (ICIP), 2010 17th IEEE International Conference on, pages 3045–3048. IEEE, 2010.
54. Khan, M. D. H., Ahmed, M., and Bach, C.: Preliminary detection and analysis of lung cancer on ct images using matlab: A cost-effective alternative. Journal of Biomedical Engineering and Medical Imaging, 2(6):01, 2016.
55. Russ, J. C.: The image processing handbook. CRC press, 2016.

CITED LITERATURE (continued)

56. Boellaard, R., O'Doherty, M. J., Weber, W. A., Mottaghy, F. M., Lonsdale, M. N., Stroobants, S. G., Oyen, W. J., Kotzerke, J., Hoekstra, O. S., Pruim, J., et al.: Fdg pet and pet/ct: Eanm procedure guidelines for tumour pet imaging: version 1.0. European journal of nuclear medicine and molecular imaging, 37(1):181, 2010.
57. Al Mohammad, B., Brennan, P., and Mello-Thoms, C.: A review of lung cancer screening and the role of computer-aided detection. Clinical radiology, 72(6):433–442, 2017.
58. Oppelt, A.: Imaging systems for medical diagnostics: fundamentals, technical solutions and applications for systems applying ionizing radiation, nuclear magnetic resonance and ultrasound. John Wiley & Sons, 2011.
59. Dicom. <https://www.dicomstandard.org/about/>. Accessed: 2018-04-09.
60. Senthilkumaran, N. and Rajesh, R.: Edge detection techniques for image segmentation—a survey of soft computing approaches. International journal of recent trends in engineering, 1(2):250–254, 2009.
61. Otsu, N.: A threshold selection method from gray-level histograms. IEEE transactions on systems, man, and cybernetics, 9(1):62–66, 1979.
62. Atherton, T. J. and Kerbyson, D. J.: Size invariant circle detection. Image and Vision computing, 17(11):795–803, 1999.
63. Liu, M., Yang, X., and Shang, Y.: Image quality assessment based on multi-scale geometric analysis. In International Conference on Image Analysis and Processing, pages 807–815. Springer, 2009.
64. Soille, P.: Morphological image analysis: principles and applications. Springer Science & Business Media, 2013.
65. Haralick, R. M., Sternberg, S. R., and Zhuang, X.: Image analysis using mathematical morphology. IEEE transactions on pattern analysis and machine intelligence, (4):532–550, 1987.
66. Chan, T. F. and Vese, L. A.: Active contours without edges. IEEE Transactions on image processing, 10(2):266–277, 2001.
67. General electric. <https://mind.net.au/wp-content/uploads/2017/03/PETCT-690-series-data-sheet-US-rev1.pdf>. Accessed: 2018-04-16.

CITED LITERATURE (continued)

68. Siemens. <https://ftp.siemensmedical.com/PP-Cutsheets/MI/Biograph\%20\%206/Cutsheet-04096.pdf>. Accessed: 2018-04-16.
69. Iso. <https://www.iso.org/obp/ui/#iso:std:iso:12052:ed-2:v1:en>. Accessed: 2018-04-15.
70. Canny, J.: A computational approach to edge detection. In Readings in Computer Vision, pages 184–203. Elsevier, 1987.
71. Matlab release. <https://tinyurl.com/matlab-2017b-release>. Accessed: 2018-04-16.
72. Borgefors, G., Nyström, I., and Di Baja, G. S.: Connected components in 3d neighbourhoods. In PROCEEDINGS OF THE SCANDINAVIAN CONFERENCE ON IMAGE ANALYSIS, volume 2, pages 567–572. PROCEEDINGS PUBLISHED BY VARIOUS PUBLISHERS, 1997.

VITA

NAME	Eleonora D'Arnese
EDUCATION	
Spring 2017 - On date	Master of Science in BioEngineering, University of Illinois at Chicago, USA
Fall 2016 - On date	Master Degree in Biomedical Engineering, Politecnico di Milano, Italy
Fall 2013 - Spring 2016	Bachelor Degree in Biomedical Engineering (BE), Jul 2016, Politecnico di Milano, Italy
LANGUAGE SKILLS	
Italian	Native speaker
English	Full working proficiency
	2016 - IELTS examination (8/9)
	2012 - FCE Cambridge examination (74/100)
	A.Y. 2017/18 One Year of study abroad in Chicago, Illinois
SCHOLARSHIPS	
N/A	N/A
TECHNICAL SKILLS	
Good level	Programming (C, Matlab, Python)
Good level	Image Processing
Good level	Problem Solving
EXPERIENCE	
Spring 2017	Xilinx Open Hardware Contest.
July 2016	Xilinx Pynq Hackathon.
Spring 2016	Xilinx Open Hardware Contest, EMEA Finalist.
PUBLICATIONS	

VITA (continued)

Summer 2017	A. Purgato, E. Reggiani, E. D'Arnese, T. Berger-Wolf, M. Grimaldi, G.Durelli, M. D. Santambrogio. GPU-based computation for brain spatio-temporal networks definition. <i>39th Annual International Conference of the IEEE Engineering in Medicine and Biology Society (EMBC), May 29th-30th, 2017, Jeju Island, South Korea - In Proceedings.</i>
Spring 2017	E. Reggiani, E. D'Arnese, A. Purgato, M. D. Santambrogio. Pearson Correlation Coefficient Acceleration for Modeling and Mapping of Neural Interconnections. <i>Parallel and Distributed Processing Symposium Workshops (IPDPSW), July 11th-15th, 2017, Orlando, USA - In Proceedings.</i>
<hr/>	
PROJECTS	
Fall 2017	Parkinson's disease classification Developed during the course Statistics and Machine Learning at UIC.
	Heart surgery simulation Developed during the course Haptics at UIC.
Spring 2017	BrainQube. BrainQube is a project developed at Politecnico di Milano. This work proposed a hardware implementation of ICA algorithm applied to images obtained by functional Magnetic Resonance Imaging to better identify the development process and the effects of neural pathologies.
July 2016	Die Hardware. Die Hardware is a project developed at Politecnico di Milano. It created a digital writing system based on eye tracking able to provide a mean for patients suffering from particularly debilitating diseases to communicate and interact with other people.
Spring 2016	Brain NECSTwork.. Brain NECSTwork is a project developed at Politecnico di Milano that proposed an FPGA-based implementation of the Pearson Correlation Coefficient. The aim of the project was to use such implementation for the creation of brain networks from images obtained from functional Magnetic Resonance Imaging that are used to quickly and accurately model and map neural interconnections inside human brain.
